# CHAPTER-1

# INTRODUCTION

## 1.1 INTRODUCTION-

Rock mechanics is the theoretical and applied science of the mechanical behaviour of rock and rock masses & compared to geology, it is that branch of mechanics concerned with the response of rock and rock masses to the force fields of their physical environment. This field is not associated with only the theoretical behaviour of the rock but also the design of the structure in rock like tunnel, underground structures.

Rock mechanics forms part of the broader subject of geomechanics, which is concerned with the mechanical responses of all geological materials, including soils. Rock mechanics, as applied in engineering geology, mining, petroleum and civil engineering practice, is concerned with the application of the principles of engineering mechanics to the design of the rock structures generated by mining, drilling, reservoir production, or civil construction activity, e.g. tunnels, mining shafts, underground excavations, open pit mines, oil, road cuts, waste repositories, and other structures built in or of rock. It also includes the design of reinforcement systems, such as rock bolting patterns.

It is convenient to subdivide rock mechanics into the following branches:

(a) Structural rock mechanics, which is concerned with the stability of engineering structures in which the material is predominantly rock.

(b) Comminuting, which is concerned with the reduction of rock to small fragments by the application of external forces as in drilling, blasting, cutting and grinding.

Rock is the material which may be intact or which may be in the disintegrated form. Their form has very high influence over the engineering properties .The strength is high in intact rock and very low in the jointed rock .The frequency is also a very important parameter which defines the strength of rock.

For designing any structure or analyzing rock, the characterization of material is very important in rock mechanics. The aim of this research is also to study the shear and dilation behaviour of artificial rock joint (prepared by Plaster of Paris) and to model the shear behaviour using experimental results and numerical methods.

Artificial joints have been studied mainly as they have the advantage of being reproducible for eg: Gypsum plaster has been found to be suitable for simulating the behaviour of jointed soft rocks such as coal, friable limestone, clay shale and mudstone. (Indraratna, 1990; Rao and Shrivastava, 2011). Laboratory studies show that many different failure modes are possible in jointed rock and that the internal distribution of stresses within a jointed rock mass can be highly complex. Numerical simulation of rock joints has been also been performed by researcher time to time (Haque and Indratna, 1999; Roosta et.al., 2006; Shrivastava et.al. 2012 etc) and it has been observed by them that numerical results are in close approximation to experimental results.

## 1.2 ORGANIZATION OF REPORT-

- Chapter 1: Provides the introduction to the related field and deals about need of the work.

- Chapter 2: Describes the literature review of the topic in which various model for shear , dilation behaviour and rock joint properties are discussed. Also various numerical techniques has been discussed which are available in order to simulate rock-joint behaviour.

- Chapter 3: Discuss about various test and their results performed in order to characterize the material and to study shear and dilation behaviour of rock joints.

- Chapter 4: This chapter deal with the comparison of Result obtained from Experimental work with well known theories.

- Chapter 5: This chapter consists of Conclusion and Future work which can be done for new research in the field of rock joint.

# CHAPTER-2

# LITERATURE REVIEW

## 2.1 BEHAVIOUR OF ROCK JOINT IN SHEAR-

A natural discontinuity surface in rock is never as smooth and undulations and asperities are always present in the rock on a natural joint surface. These undulation and asperities have a significant influence on the shear behaviour of the joint and generally increases the shear strength of the surface. Compared to intact rocks jointed or fractured rock mass shows high permeability, higher deformation characteristics and low shear strength along the plane of discontinuity. Thus the study of strength parameters becomes very important for the analysis of effect of joints on rock mass. In case of rough joint surfaces shear displacement is accompanied by vertical displacement.

### 2.1.1 Patton Shear Strength Criteria (1966) -

Patton in 1966 demonstrated the influence of roughness by means of shear test carried out on 'saw-tooth' specimens. According to Patton shear strength of saw-tooth specimens is represented by:

$$\tau_p = \sigma_n \tan(\phi_b + i) \quad \text{for low normal stress} \tag{1}$$

$$\tau_p = c_o + \sigma_n \tan(\phi_b) \quad \text{for high normal stress} \tag{2}$$

Where, $\Phi_b$ is the basic frictional angle, $i$ is initial asperity angle, $c_0$ is cohesion intercept

### 2.1.2 Ladanyi and Archambault Shear Strength Criteria (1970) –

According to Ladanyi and Archambault Peak Shear Strength is given by:

$$\tau_p = \frac{\sigma_n (v + \tan\phi_b)(1 - a_s)(a_s s_r)}{1 - (1 - a_s) v \tan\phi_b} \tag{3}$$

Where, $a_s$ and ν are the proportion of total joint area sheared through the asperities and the rate of dilatancy at the peak shear strength respectively and $s_r$ is the shear strength of the rock comprising the asperities. Both $a_s$ and ν are dependent on normal stress and are given by following relationship.

$$a_s = 1 - (1 - \frac{\sigma_n}{\sigma_T})^{k_1} \tag{4}$$

$$v = 1 - (1 - \frac{\sigma_n}{\sigma_T})^{k_2} \tan i_0 \tag{5}$$

Where, $k_1$ and $k_2$ are empirical constants with suggested values of 1.5 and 4 respectively and $\sigma_T$ is the transitional stress (Saeb & Amadei in 1992) modify Ladanyi and Archambault criteria. Their criterion led emphasis on the simultaneous contribution of shearing and sliding to the shear strength of a rock joint. In above equation $a_s$ is the proportion of joint surface area sheared through the asperities and (1-$a_s$) is the proportion on which sliding occurs. The relative contribution of shearing and sliding depends on the of normal stress and generally at low normal stresses it has been observed that sliding is dominant while at high normal stresses asperity shearing is dominant.

### 2.1.3 Barton's Shear Strength Criteria (1973) –

This theory is better than the Patton's theory because Patton's equation is valid at low normal stresses where shear displacement is due to sliding along the inclined surfaces while at higher normal stresses, the strength of the material get be exceeded and the teeth tend to break off which results in shear strength behaviour which is more closely related to the intact material strength than to the frictional characteristics of the surfaces. Barton (1973-1976) studied the behaviour of natural rock joints and proposed the Patton's equation in new form:

$$\tau = \sigma_n \tan(\phi_b + JRC \log_{10}(\frac{JCS}{\sigma_n})) \tag{6}$$

Where, JRC is joint roughness coefficient and ranges from 0-20

JCS is joint compressive strength and depends on $\sigma_c$

### 2.1.4 Shear Strength Behavior of Rock Proposed by Shrivastava and Rao (2010), Shrivastava and Rao (2011),Shrivastava et. al, (2012) ,Shrivastava and Rao (2013)–

Shear strength of rock under CNL condition can be given by –

$$\sigma_n = tan(\phi_b + i') \tag{7}$$

Where $\phi_b$ is the Basic friction angle

i' is effective asperity angle ,given by

$$i' = \left[ c\, e^{-d\frac{\sigma n}{\sigma c}} \right] i \qquad (8)$$

Where c and d are constant whose values depends upon the angle of asperity sample.

**Table No.1:** Shows the values of c and d

| Asperity | c | d |
|---|---|---|
| $15^{\circ}$-$15^{\circ}$ | 1.796 | 4.98 |
| $30^{\circ}$-$30^{\circ}$ | 1.301 | 6.54 |

## 2.1.5 Shear Behaviour of Rock Joints under Cyclic Loading (2012) –

This study shows a systematic way of investigation carried out on the cyclic shear behaviour of artificial rock joints under CNS conditions (Homand, F., Lefevre, F., Belem, T., Souley, M., 1999).The following conclusion are obtained-

1-Generally expected, cyclic shear behaviour of rock joints changes from asperity slidding to asperity shearing with increasing shear stress.

2-Due to the damage of asperity, the shear strength diminishes with increasing number of shear cycles.

3-Degradation of asperities mostly occurs at the initial cycles and attenuates with increasing numbers of shear cycles.

4-By increasing the applied normal stress and the number of shear cycle, contracting (seating) may be observed rather than dilatancy behaviour.

5-Cyclic peak shear strength under CNL condition is obtained at greater cyclic shear displacement rather than that of the CNL condition.

### 2.1.6 Rock Dilation on Modeling Failure and Deformation of Hard Rocks (Xingguang Zhao, Meifeng Cai, M.Cai 2010) –

Based on a practical case of the mine by test tunnel in URL in CANADA, the influence of rock mass dilation on the brittle failure and deformation of the tunnel is investigated using the empirical dilation angle model ,which consider the influence of plastic shear strain and confinement .The main achievement and conclusion are drawn-

1- For the given rock mass and the boundary conditions, different excavation methods lead to different stress paths, which have an important impact on the failure modes around the excavation boundaries .In numerical modeling, the behaviour of rock mass can be reasonably revealed only when the stress path in the rock mass is captured correctly.

2- For modeling brittle failure of rock mass, the conventional models such as perfectly elasto-plastic, strain softening model and elasto-brittle-plastic model cannot predict failure zone that matches the shape observed V-shapes notch .The three models underestimate the depth of shear failure in the roof and floor of the tunnel and overestimate the extent of lateral failure.

3- From Numerical simulation results that the confinement and the plastic shear strain dependent dilation angle model proposed by them can reasonably describe both the rock mass failure and the displacement distribution near the excavation boundary simultaneously The predicted failure shape of the tunnel and the rock mass displacement distributions induced by the gradual excavation are in good agreement with the field measurement results. The presented study result provides a useful approach to understand the nonlinear mechanical behaviour of rocks and to investigate the rock dilation near the excavation at depth.

## 2.2 DILATION BEHAVIOUR OF ROCK-

### 2.2.1 Introduction-

The term Dilation ($\delta_v$) can be defined as the relative moment between two joint faces along the profiles. In direct shear test, dilation is defined as the relative movement between the planes during testing. In this study dilation is only the vertical displacement and hence should not be misinterpreted with the volumetric strain ($\varepsilon_v$) which is also referred as dilation in Triaxial Test.

Dilation can be represented in form of dilation angle as follows:

$$\tan d^{\circ} = \frac{\delta_v}{\delta_h} \tag{9}$$

Where the symbols have their specific meaning $d^{\circ}$ is the dilation angle, $\delta_v$ is vertical displacement and $\delta_h$ is horizontal or shear displacement in mm.

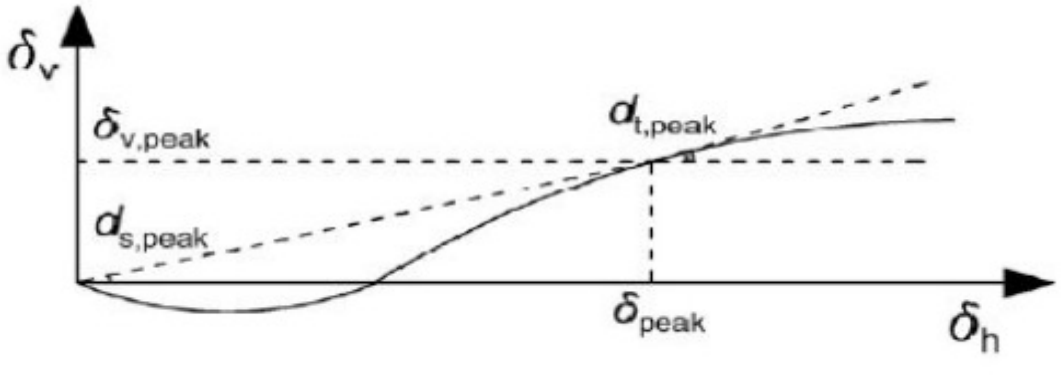


**Fig 2.1:** Showing variation of shear displacement- dilation curve
(courtesy: Asadollahi, P., Tonon F., Invernizzi, M.C.A, Addotto, S. 2010, "experimental validation of modified Barton's model for rock fractures" Rock Mech Rock Eng.)

$$d_{s,peak} = \tan^{-1}\left(\frac{\delta_{v,peak}}{\delta_{peak}}\right) \tag{10}$$

According to this theory peak tangent dilation angle is represented by $d_{t,peak}$ and given by:

$$d_{t,peak} = \left(\frac{\partial \delta_v}{\partial \delta_h}\right)_{at \delta_h = \delta_{peak}} \tag{11}$$

## 2.2.2 Model of Ladayani and Archambault (1970)-

Ladayani and Archambault in 1970 proposed the following relation to determine peak tangent dilatancy

$$\tan i_p = (1 - \frac{\sigma_n}{\sigma_T})^{k_2} \tan i_{po} \tag{12}$$

Where, $k_2$ is an empirical coefficient influenced by joint surface roughness and having values in range between 0.25 and 3.55, tan ($i_{po}$) is the peak rate of dilatancy at zero normal stress.

### 2.2.3 Barton and Choubey (1977)-

According to them -1) Both Peak and initial dilation angles were occasionally negative or zero . In such cases the joints did not start to dilate significantly until after peak strength was reached, and in fact may have contracted. When this type of dilation occurs in spite of a quite high asperity component, it signifies that the joint "failed" when a small steep interlocking projection failed.

2) They found that peak secant dilation angle is equal to the difference between the measured total friction angle ($\tan^{-1}\tau_p/\sigma_n$) and the estimated residual friction angle ($\Phi_r$) and they also showed that peak secant angle is about one-third of the peak tangent dilation angle.

3) According to him the range of peak dilation angle is given by

$$0.5\ JRC\ \log_{10}(JCS/\sigma_n) < d_{t.peak} < 2\ JRC\ \log_{10}(JCS/\sigma_n) \tag{13}$$

4) They give the following relationship to estimate the peak secant and tangent dilation angles

$$d_{t,peak} = JRC.\log_{10}(\frac{JCS}{\sigma_P}) \tag{14}$$

$$d_{s,peak} = \frac{1}{3} JRC.\log_{10}(\frac{JCS}{\sigma_n}) \tag{15}$$

5) They then introduce the factor 'M' known as damage coefficient such that

$$m = \frac{JRC}{12\log_{10}(JCS/\sigma_n)} + 7.0 \tag{16}$$

Value of M can also be taken as 1 or 2 for shearing under low or high stress respectively (Olsson and Barton, 2001). The value of peak tangent dilation angle can then be corrected by dividing it

by the factor M. Barton in 1982 state that dilation will begin when $JRC_{mobilized} = 0$ and in that case mobilized tangent dilation angle, $d_t$ can be estimated from the following relationship.

$$d_{t,mobilized} = \frac{1}{m} JRC_{mobilized}.\log_{10}(\frac{JCS}{\sigma_n}) \tag{17}$$

Where

$$JRC_{mobilized} = \frac{\tan^{-1}(\tau(\delta_h / \sigma_n)) - \phi_r}{\log(JCS/\sigma_n)} \tag{18}$$

Asadollahi in 2010 has give the equation for peak secant dilation angle which gives good result

$$d_{s,peak} = \tan^{-1}(\frac{1}{3}\tan(JRC.\log(\frac{JCS}{\sigma_n}) \tag{19}$$

He also proposed an empirical model for pre-peak dilatancy behaviour of rock fractures and dilation displacement can be calculated at each shear displacement using this equation. Also this model does not contain any of the inconsistencies and ambiguity of Barton's model.

$$\frac{\delta_v}{\delta_{peak}} = \frac{1}{3}\tan(JRC.\log(\frac{JCS}{\sigma_n})).(\frac{\delta_h}{\delta_{peak}}).(2(\frac{\delta_h}{\delta_{peak}}) - 1) \tag{20}$$

## 2.3 PEAK SHEAR DISPLACEMENT IN ROCKS –

It has been explained earlier that peak shear displacement is the horizontal displacement required to reach peak shear strength. Bandis et. al. (1981) indicated that $\delta_{peak}$ is generally about 1% of the joint sample length (L). For example in case of laboratory-size samples ( $L_0$ = 100 mm), during shearing first 1 mm of shear displacement $\Phi_r$ is mobilized first, and then roughness, causing post-peak dilation, at displacements larger than our example 1mm, roughness is gradually destroyed or work down and dilation continues but at a reduced rate post-peak. Bandis et. al (1981) suggested a relation to estimate the value of $\delta_{peak}$ from the analysis of 650 shear test. He also investigate that the $\delta_{peak}$ is dependent on the dimension of sample taken (L in meters) and the roughness JRC of the sample and he suggested:

$$\frac{\delta_{peak}}{L} = \frac{1}{500}\left(\frac{JRC}{L}\right)^{.33} \tag{21}$$

L and $\delta_{peak}$ are in meters

Barton in 1982 relates the ratio of $JRC_{peak}/JRC_{mobilized}$ with the ratio of $\delta_h/\delta_{peak}$ .

Asadollahi in 2010 proposed an equation for the prediction of peak shear displacement based on the regression analysis of about 317 samples. Equation has been found good in predicting peak shear displacement compared to the Barton's equation. The equations are for joints

$$\delta_{peak} = 0.007 L^{0.45}\left(\frac{\sigma_n}{JCS}\right)^{0.34} \cos\left(JRC \log\left(\frac{JCS}{\sigma_n}\right)\right) \tag{22}$$

Where, L is length of the block is in meters and $\delta_{peak}$ is also in meters.

## 2.4 NUMERICAL METHODS IN ROCK ENGINEERING –

Numerical method of Analysis can be distinguished in following ways continuum method, discontinuum method and hybrid method (Jing and Hudson, 2002).

In continuum method rock mass is treated as a continuous material. In this method the problem domain is divided into finite number of elements and than their behaviour is approximated by simpler mathematical equations. These elements must satisfy governing equations and compatibility condition at interfaces with adjacent elements (L. Jing, 2003; Jing and Hudson, 2002). In the continuum approach plastic softening and damage models are most common techniques for capturing failure and localization . The most commonly applied methods based on continuum approach are finite element method (FEM), finite difference method (FDM), boundary element method (BEM).

In continuum method rock mass is treated as a continuous material. In this method the problem domain is divided into finite number of elements and than their behaviour is approximated by simpler mathematical equations. These elements must satisfy governing equations and compatibility condition at interfaces with adjacent elements (L. Jing, 2003; Jing and Hudson, 2002). In the continuum approach plastic softening and damage models are most common techniques for capturing failure and localization. The most commonly applied methods

based on continuum approach are finite element method (FEM), finite difference method (FDM), boundary element method (BEM).

In discontinuum method Rock is represented as a discontinuous mass. Blocky nature of system is analyzed and it is assumed that block may interact with neighboring block through the joints and special emphasis is devoted for the characterization of rock element, rock joint and discontinuities (Barla et.al, 1999). The most important methods based on this approach are distinct element method and discrete fracture nature method (DFN).

Continuum methods may include the discontinuities in the medium if present, explicitly or implicitly, while in discontinuum methods discontinuities are included explicitly. There is no quantitative guideline for the suitability of one method over other. The choice of continuum or discontinuum method depends on highly on the problem scale and fracture system of geometry, In general the continuum approach can be used if only few fractures are present and complete block detachment are not significant factors and discontinuum approach is suitable for moderately fractured rock masses or where large-scale displacement of individual blocks are possible (Jing,2003) .A pseudo continuous displacement field is assumed to be formed if medium is heavily jointed such that the blocks defined by discontinuities have a size much smaller than the opening, and in such cases use of continuum model seems reasonable (Bobet.et.al, 2009).

The disadvantage of each method can be avoided by combined continuum and discontinuum models. Basic approach is to model far-field as isotropic continuum using BEM and the near-field fractured rock by using either DEM or FEM and combinations are FEM/BEM, BEM/DEM, and FEM/DEM.

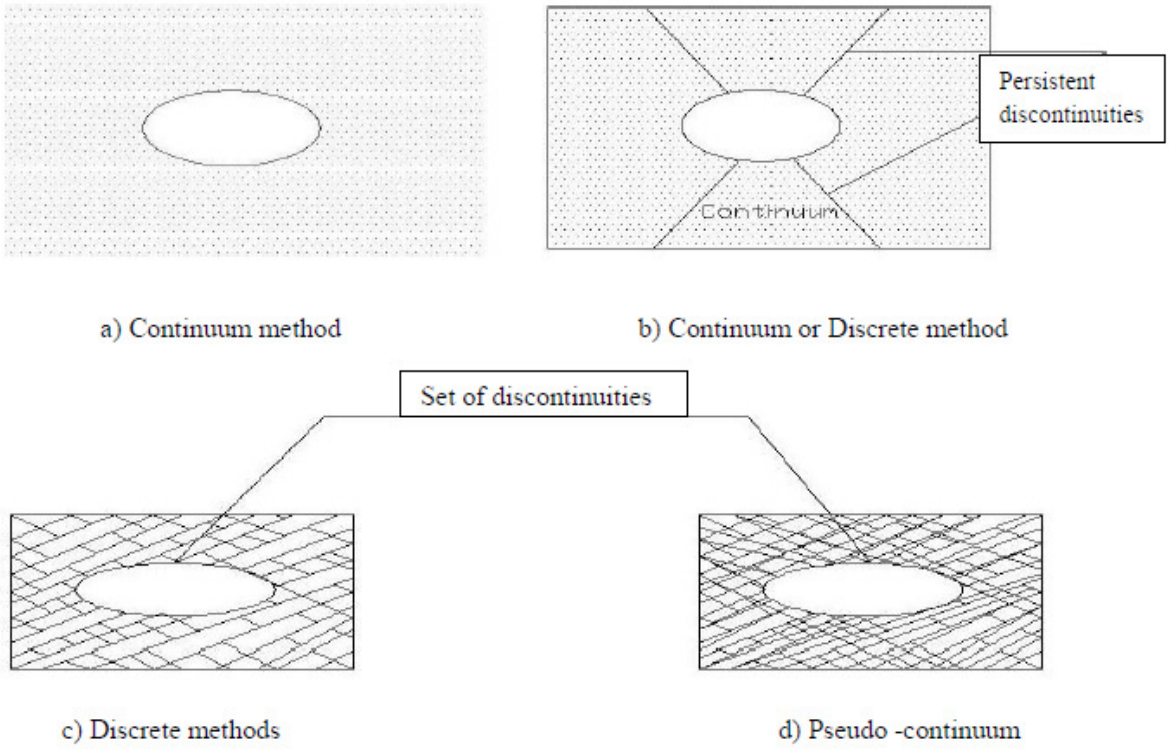


**Fig 2.2:** Shows the suitability of different methods of Excavation in a Rock mass

(Courtesy: L.Jing 2003, "A review of techniques, advances and outstanding issues in numerical modelling for rock mechanics and rock engineering" Elsevier)

### 2.4.1 The FDM and Related Methods-

The basic technique in the FDM is discretization of the governing PDE's by replacing the partial derivative with the differences at neighboring gird points. The solutions for the system equation are obtained by imposing necessary initial and boundary conditions. The continuum is represented by a series of discrete grid point at which displacements, velocities and accelerations are calculated. The displacement field is computed by approximating the differential equations for the system as a set of difference equations (central, Forward or backward) that are solved discretely at each grid point. The differential equations are approximated through the use of difference equations (Jing and Hudson, 2002; Jing, 2003).

Grid system is a convenient way generating objective functional values at sampling points with small interval between them, so that errors incurred will be small and acceptable. The

formation and solutions of the equations are localized, which is more efficient for storage handling in computer implementation. It is the most direct and interactive technique for the solutions of PDE's and also provides the additional advantage of direct simulation of complex material, such as damage and plasticity.

According to (Perrone and Kao, 1975), in FDM irregular meshes, such as quadrilateral gird are generated and these grids enhance the applicability of the FDM for rock mechanics problems. This approach is so called Finite volume method. For unstructured grid, the FVM is formulated at nodes (grid points) or at the center of the elements with the help of displacement variable. It has similarities with the FEM and act as a bridge between the FDM and FEM.

The most well known computer code using for stress analysis for rock engineering problems using the FVM/FDM approach is the FLAC code group (ITASCA Consulting Group, Inc. FLAC Manual). Representation of fractures is not easy in the FDM/FVM because they require the continuity of the grid points. On the other hand, FDM/FVM models have been used to study the mechanisms of fracturing processes, such as shear formation in the lab testing of rock and soil samples. The FVM is one of the most popular methods in rock engineering, covering all aspects which are related to Rock mechanics such as Slope stability, underground openings, and hydro mechanical or thermal hydro mechanical process.

### 2.4.2 The FEM and Related Methods-

In FEM domain discretization involves dividing the domain into the number of sub domain of standard shapes (Triangular, Tetrahedral and Quadrilateral) with fix number of nodes at vertices and on the sides. Polynomial functions are generally used as trial functions in order to approximate the behaviour of PDE at element level and by generating local algebraic equations for representing the behaviour of elements. The elements equations are categorized according to the topological relation between nodes and elements and then assembled in to global system of algebraic equation, the solution that provides the required information in the solutions domain.

As this model is based on continuum assumptions, block rotation, sliding, large scale opening and complete detachment are not permitted and formulation of FEM requires that fractured or jointed elements cannot be torn apart (Jing and Hudson 2002).

Due to its flexible approaches in handling material heterogeneity and anisotropy, complex boundary conditions and dynamics problems makes FEM, one of the best popular numerical method. In order to counter the material in homogeneity in FEM different materials properties are assigned to different elements. In order to consider the effect of an infinite far-field domain on the near –field behaviour 'infinite domain element" has been developed in FEM (Beer and Meck 1981).Many computer codes has been generated based on FEM of which PLAXIS, PHASE-2, and ABQUAS are most popular.

Treatment of fractures and fracture growth is the most important factor which limits the application of FEM in rock mechanics. Requirement of small element size, continuous remeshing with fractures and conformable fracture path and elements edge for simulating the fracture growth process make FEM inefficient in dealing with such fractured rock mass problem.

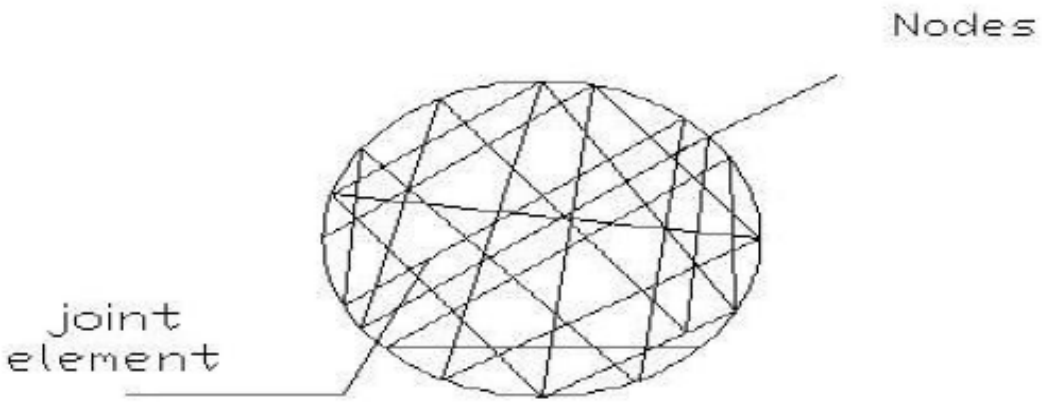


**Fig 2.3:** Shows the Fractured Rock by FEM method
(Courtesy:http://weikipedia/Representation of fractured rock by FEM)

### 2.4.3 The BEM and Related Methods-

Initially BEM approach seeks a weak solution of an integral equation which is derived using Betti's Reciprocal theorem. The introduction of isoparametric elements using different orders of shapes function greatly enhanced the BEM's applicability for stress analysis problems.

This method derives its name from the fact that the user 'discretizes' or divides into elements, only boundaries of the problem geometry (i.e. excavation surfaces, the free surface for shallow problems, joint surfaces and material interfaces) thus reducing the problem dimensions by one and greatly simplifying the input requirements. In this method the conditions on a surface could be related to the state at all points throughout the remaining medium, even to infinity. The information required in the solution domain is separately calculated from the information on the boundary, which is obtained by solution of boundary integral equation.

In order to simulate the fracture growth using BEM, two techniques are used. First is to divide the problem domain into multiple sub domains with fractures along with their interfaces, with a pre-assumed fracture path. Second is the dual boundary element method (DBEM) using displacement.

Input data preparation is comparatively is generally simpler in case of BEM as simpler mesh are generated with decreased model reduction. But BEM is not as efficient as FEM in dealing material heterogeneity as it does not contain many sub-domains as contained by an element in FEM. BEM is also not efficient for simulating non-linear material behaviour. According to Jing and Hudson, BEM has been found more suitable in case of problems related to fracturing of inhomogeneous and linearly elastic bodies, stress and deformation analysis for underground excavations, soil-structure interaction, groundwater flow and fracturing processes and some of its uses are as: 1) Structure analysis of underground excavations with and without fracture; 2) Dynamic Analysis; 3) Elastic properties; 4) Borehole tests for permeability measurements.

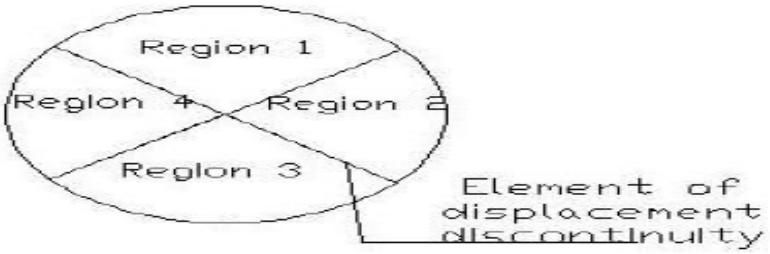


**Fig 2.4:** Representation of Fractured Rock by BEM

(Courtesy: L.Jing 2003,A review of techniques, advances and outstanding issues in numerical modelling for rock mechanics and rock engineering. Elsevier)

### 2.4.4 The DEM and Related Methods-

DEM is a Lagrangian numerical technique where the computational domain consists of discrete solid elements that interact via compliant contacts (Bobet et.al, 2009*).* Basic concept of DEM is that the domain of interest is generally treated as an assemblage of rigid or deformable blocks and contact information among each block is identified and updated continuously during the deformation process.

The theoretical foundation of the method is to derive and solve the equation of motion of rigid or deformable blocks using implicit (based on FEM discretization) and explicit (based on FDM/FVM discretization) formulation. It has been assumed in DEM that discontinuities divide the medium and bound finite number of blocks through their intersection. These blocks are in turn interconnected through the discontinuities. Three main issues which are needed to be addressed by DEM are (Cudall and Hart, 1992; Jing, 2003): 1) Representation of contacts i.e. identification of blocks or particle system based on the fracture geometry or on the particle shape assumption within the domain 2) Formulation and solution of equation of motion representing the behaviour of particle system 3) Detecting and continuously updating the contact information during the execution of discrete system. The main difference between DEM and continuum based methods is that the contact pattern is fixed in continuum approach while continuously changing and updating in DEM. The explicit representation of fractures makes DEM, most attractive and suitable method for rock mass modeling. Many explicit computer codes has been developed based on DEM approach, UDEC and 3-DEC are two such computer codes for two and three dimensional problems in rock mechanics (ITASCA Consulting Group). Though DEM as is flexible and powerful tool for analyzing discontinuous rock but difficulty associated in obtaining reliable data on location, orientation and persistence of discontinuities, lack of information on material behavior limits its application. But in general it remains as qualitative and useful tool for deformation analysis of fractured blocky rock mass and also provides an insight into failure mechanism.

***Discontinuous deformation analysis (DDA) -*** This is the method of representing implicit DEM. It was first formulated by Shi and Goodman 1984, 1985 and was further developed for stress deformation analysis, and for coupled stress-flow problem. According to Jing and Hudson (2002)

and Jing (2003) DDA method uses standard FEM meshes over blocks and contacts are treated using penalty method. According to Shi (1988) medium is discretized into elements or blocks that are in contacts with each other only through their boundaries.

DDA has two main advantages over explicit DEM: 1) relatively larger time steps and closed-form integration for stiffness matrices of elements 2) an existing FEM code can also be readily transformed into a DDA code while retaining all advantageous features of FEM.

***Discrete Fracture Network (DFN) –***This method is a special discrete model which was created in early 1880s for both two and three dimensional problems. DFN model considers fluid flow and transport processes in fractured rock masses through a system of connected fractures flow. Its application is found for the study of flow in fractured media, for the derivation equivalent continuum and transport properties of rock. The basis of DFN model is the knowledge, understanding and representation of fracture system geometry and transmissivity of individual fractures (Jing. 2002), hence like in DEM, stochastic simulation of fracture system also plays an important role in the performance and reliability of DFN model.

Due its conceptual attractiveness it has find many application for modeling of fractured rock mass problem. The main computers codes based on DFN approach are FRACMAN/MAFIC and NAPSAC.It is difficult to model the effects of mechanical deformation and heat transfer on fluid flow in DFN also lack of knowledge of geometry of rock fractures limits its application.

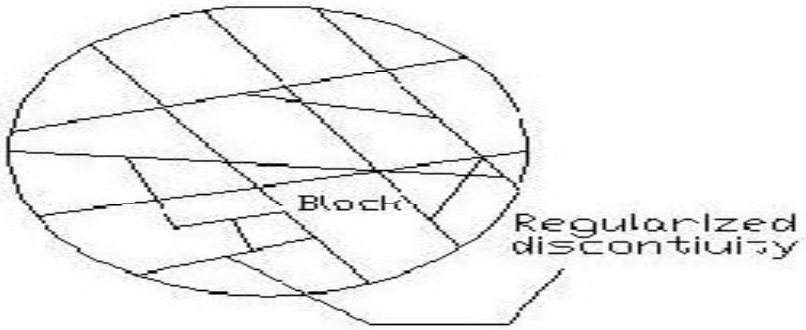


**Fig 2.5:** Representation of a fractured rock mass by DEM

(Courtesy: L.Jing 2003 "A review of techniques, advances and outstanding issues in numerical modeling for rock mechanics and rock engineering". Elsevier)

### 2.4.5 Methods Related With Hybrid Model –

This method is based on continuum and discontinum approaches both .The main types of hybrid models are FEM/BEM, BEM/DEM and FEM/DEM. In this method it is assumed that the far field Rock behaves as the elastic quatinum and near-field is assumed as fractured and non-linear in behaviour hence requires explicit representation of fractures. Commonly BEM is used for simulating far-field and FEM and DEM is used for near-field .Hybrid models are being frequently used in rock engineering for flow and stress/deformation problem (Jing. 2003).

***Hybrid FEM/BEM models*** method was presented as a stress analysis technique by Brady and Wassyng (1981). It has found its application for simulating the mechanical behaviour of underground excavations.

***Hybrid DEM/BEM models*** was implemented only for the explicit DEM, referred to the code group of UDEC and 3-DEC. It is technique which is created by Lorig and Brady (1982, 1984, 1986), and implemented in UDEC. The basic concept is to treat the far-field BEM region as a super block region having contacts with smaller blocks along the interfaces with near-field DEM region.

***Hybrid DEM/FEM models*** is the one in which the DEM region consists of rigid blocks and FEM region consists of material having non-linear behaviour. Though hybrid models are very useful, special attention needed for continuity or compatibility condition at the interfaces between regions of different model (Jing, 2003).

## 2.5 UNIAXIAL COMPRESSIVE STRENGTH (UCS) ON ROCK-

Uniaxial compressive strength of rock can be determined from Schmidt Hammer Test, Point Load Test and Unconfined Compression Test.

The Schmidt Hammer is a simple device for recording the rebound of a spring loaded plunger after its impact with a surface. The L-hammer used generally for experimental study (impact energy =0.075 m kg) is suitable for testing small and impact-sensitive parts of concrete and artificial rocks. It is suitable for measuring UCS values of about 20 MPa to 300 MPa.

Miller in 1965 gives an empirical equation for rebound number ranging from 10 to 100 and uniaxial compressive strength ($\sigma_c$) of rock.

$$\log_{10} \sigma_c = 0.0088\gamma R + 1.01 \tag{23}$$

Where, $\sigma_c$= Uniaxial compressive strength of surface in MPa; $\gamma$ =dry density of rock (KN/m$^2$) and R = Rebound number.

Uniaxial compressive strength of a rock sample can also be calculated from Point Load Strength as suggested by ISRM (1985). The point load index is defined as:

$$I_s = \frac{P}{D^2_e} \tag{24}$$

Where, $D_e$ is the equivalent core diameter in mm

For non-circular cross-sections $D_e = \sqrt{\frac{4A}{\pi}}$ in which A is the minimum cross-sectional area of a plane trough the specimen (Asadollahi et.al). The values Is, should be modified for diameter corrections:

$$I_{(s)50} = FI_{(s)} \tag{25}$$

$$F = (D_e / 50)^{0.45} \tag{26}$$

According to ISRM suggest that uniaxial compressive strength is about 20-25 times of point load index.The uniaxial compression test measures the unconfined compressive strength, Young's modulus, and poisson ratio of rock material.

## 2.6 JOINT WALL COMPRESSION STRENGTH (JCS) OF ROCK –

According to Barton, measurement of JCS is of fundamental important since it is largely the thin layers of rock adjacent to joint walls that control the strength and deformation properties of the rock mass as a whole. The value of JCS varies according to the weathering condition of joints. The depth of penetration of weathering into joint walls invariably depends on rock type and permeability of rock. The weathering process of a rock mass can be summarized in the following simplified stages (Barton and Choubey, 1976):

1) Formation of joint in intact rock, JCS value same as $\sigma_c$ since no weathering.
2) Slow reduction of joint wall strength if joints are water-conducting JCS< $\sigma_c$.

3) Intermediate stage weathered, water conducting joints, impermeable rock blocks between, JCS some fraction of $\sigma_c$.
4) Penetration of joint weathering effect into rock blocks; progressive reduction of σc from the walls of the blocks inwards, JCS continues to reduce slowly.
5) Advanced stage of weathering; more uniformly reduced $\sigma_c$ finally drops to same level as JCS, rock mass permeable throughout. In general if no direct measurement are available (Barton, 1973) then

   For unweathered joint: JCS= $\sigma_c$

   For weathered joint: JCS= $\sigma_c$ /4

## 2.7 JOINT ROUGHNESS COEFFIECIENT (JRC) OF ROCK –

Surface roughness of joint plane can also be quantified using a Joint Roughness Coefficient Index (*JRC*) introduced by Barton and Choubey (1976). The JRC varies between 0 and 20 and is obtained by comparing the discontinuity roughness profile to a series of reference profiles given by Barton and Choubey (1977) shown on the next page.

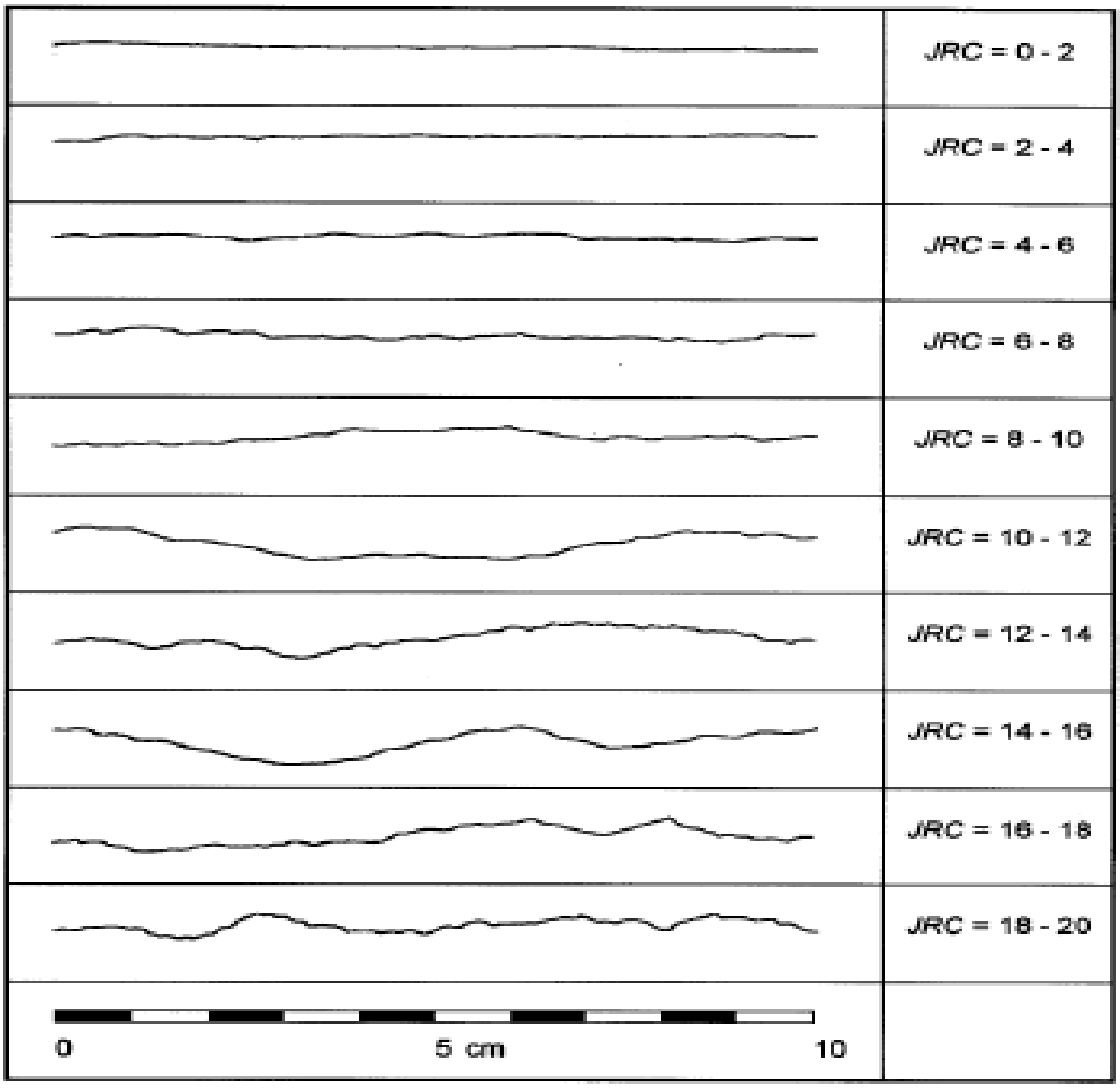


**Fig 2.6:** Shows JRC values based on Roughness Profile(After Barton and Choubey 1977)

JRC can also be estimated by Tilt test on rough surface with Schmidt hammer index test, and Tilt test on saw tooth rock surface. This is an indirect method in order to estimate the JRC:

$$JRC = \frac{\alpha^{\circ} - \phi_r}{\log_{10} \frac{JCS}{\sigma_{no}}} \tag{27}$$

where, $\alpha^{\circ}$ is the tilt angle, $\Phi_r$ is the residual friction angle, $\sigma_{no}$ is the normal stress acting on joint at tilt failure.

## 2.8 EFFECT OF SCALE ON JRC & JCS VALUES OF ROCK –

After reviewing various literatures and conducting appreciable amount of testing of joints, joint replicas, Barton and Bandis (1982) proposed the scale corrections for JRC and JCS defined by the following relationship:

$$JRC_n = JRC_0 \left(\frac{L_n}{L_0}\right)^{-0.2 JRC_0} \tag{28}$$

$$JCS_n = JCS_0 \left(\frac{L_n}{L_0}\right)^{-0.3 JCS_0} \tag{29}$$

where $JRC_o$, $JCS_o$ , $L_o$ (length) refer to 100 mm laboratory scale samples and $JRC_n$, $JCS_n$ and $L_n$ refer to in situ block sizes. There is a greater possibility of weaknesses in a large surface, and average joint wall compressive strength (JCS) may decreases with increasing scale (Barton and Bandis, 1982).

## 2.9 JOINT STIFFNESS CHARACTERSTICS –

Joint stiffness parameters describe the stress-deformation relationship of the joint. They are fundamental properties of rock joint and extremely important in the numerical modeling of jointed rock. Joint shear stiffness and joint normal stiffness are being discussed:

### 2.9.1 Joint Shear Stiffness ($K_s$)-

Joint Shear Stiffness is defined as the average gradient of the shear stress-shear displacement curve for the section of the curve below peak strength (Barton, 1972). It can be measured from the result of direct shear test and its value varies with size of the sample tested and also increases with an increase in normal stress (Bandis et al.1983).

Barton & Choubey (1977) suggested the following equation for the estimation of the peak shear stiffness (MPa/m):

$$k_s = \frac{100}{L_x} \sigma_n \tan\left(JRC \log_{10}\left(\frac{JCS}{\sigma_n}\right) + \phi_r\right) \tag{30}$$

Where, $L_x$ is the joint length in meter. This equation is based on the assumption that the peak shear strength is reached after the shearing of approximately 1% of the joint length.

## 2.9.2 Joint Normal Stiffness ($K_n$)-

Joint normal stiffness is defined as the normal stress per unit closure of the joint. Joint normal stiffness is influenced by the following factors (Bandis et al. 1983):

i) The initial actual contact area;

ii) The joint wall roughness;

iii) The strength and deformability of the asperities; and

iv) The thickness, type and physical properties of any infill material

Bandis et.al (1983) suggested the following equation for the estimation of normal stiffness

$$K_n = K_{ni}\left[1-\frac{\sigma_n}{V_m K_{ni}+\sigma_n}\right]^{-2} \tag{31}$$

Where, $V_m$ is joint maximum closure;

$K_{ni}$ is initial joint stiffness and can be obtained by:

$$K_{ni} = -7.15+1.75JRC+0.02\left(\frac{JCS}{a_j}\right) \tag{32}$$

& $a_j$ is initial joint aperture in mm under self weight such that:

$$a_j = \frac{JRC}{5}(0.2\frac{\sigma_c}{JCS}-0.1) \tag{33}$$

# CHAPTER-3

# EXPERIMENTAL WORK

## 3.1 EXPERIMENTAL WORK-

Experimental work consists of characterization of material and conventional direct shear test under constant normal load condition (In this the Normal stress is kept constant during entire process of test) .Material characterization of Plaster of Paris is done in which UCS test, Specific Gravity Test, Initial Setting Time, Final setting Time test are performed and then finally direct shear test is performed.

### 3.1.1 Materials Used-

It is very difficult to obtain the core of rock sample in field and conducting experiments on it, therefore behaviour of rock joints is simulated by molding artificial rock joints using some model material. Model material should be such that uniform, identical and homogeneous joint specimen can be prepared in order to understand the failure mechanism, deformation behaviour and strength of rock joints. It has been observed that the POP is the best material for the preparation of the artificial rocks sample.

POP is a type of building material obtained from Gypsum plaster ($CaSO_4.0.5H_2O$) hemihydrates by heating gypsum at a temperature of about 300°F. It can be easily molded into any shape when mixed with water, and the long-term strength is independent of time once the chemical hydration is completed. It has been found suitable for simulating the behaviour of jointed soft rocks such as coal, friable limestone, clay shale and mudstone. In this study material characterization of Plaster of Paris has been done. Plaster of Paris of **Sakrani Brand** has been used for this study.

### 3.1.2 Preparation of Specimens-

A bag (20 kg) of POP is available in local market. The Plaster of Paris is in powder form and is produced by pulverizing partially burnt gypsum which is duly white in color with smooth feel of cement. The water content for testing is 30%, 40%, and 50% by weight of Plaster .Initial and final setting time for each of this water content is determined and unconfined compression test are carried on intact samples prepared for the three water content is carried out after 7 days of air curing. After the analysis of test result and experience obtained during testing, it has been observed that though uniaxial compressive strength for 30% and 40% water content is higher

than that of 50% water content but initial setting and final setting time is low for them, also workable mixture is not obtained for them and molding of sample is difficult for 30% and 40% compared to 50% water content. Hence 50% water content has been finally selected for sample preparation for further study. For preparation of specimen Plaster of Paris is mixed thoroughly with 50% (by weight) water to form a uniform paste. The Plaster of Paris specimens are prepared by pouring the plaster in the mould and continuously tamping and shaking for approximately 2-3 min for proper compaction and to avoid presence of air gaps. After that it is allowed to set for 5 min and after hardening, the specimen was extruded manually from the mould and left for curing.

### 3.1.2.1 For UCS Test-

Sample for unconfined compressive test is prepared according to ISRM and IS 2720 Part 10-1991. UCS mould is hollow cylinder with length to diameter ratio greater than 2 (L/D > 2). The standard length or height of the mold was 76 mm and diameter was 38 mm having cross-section area of 1134.11 $mm^2$. Before starting sample preparation, standard mould is thoroughly oiled in inner surface so that sample can be easily taken out from the mould. For preparation of specimen, 200 gm of Plaster of Paris is mixed thoroughly with 100 ml (50% by weight) water to form a uniform paste. This paste is than poured in the standard mould with continuous shaking and tamping during pouring. After that it is allow for drying and then it is taken out slowly. The samples are than allowed to dry out in air for 7 and 14 days.

### 3.1.2.2 For Direct Shear Test –

For preparation of samples for direct shear test two moulds of size 60mm x 60mm x 25mm are casted with mild steel. For making joints, two sheets made up of plastic of thickness approximately 0.5 mm are molded in the form of continuous and uniform joint pattern with angle $15^{\circ}$-$30^{\circ}$ and $15^{\circ}$-$45^{\circ}$ and $45^{\circ}$-$15^{\circ}$ asperity sample. Inner surface of mould are oiled properly with Lubricating oil. Uniform paste of plaster is formed. During preparation of jointed sample firstly one block is casted with joint pattern sheet at the bottom. Once this sample block is fully set then it removed out from the mould and then it is inverted with joint pattern sheet and oiling is done on the surface of sheet and other metal block is kept on their top and plaster paste is than poured in it with continuous shaking for better compaction and avoid air entrapping. After setting,

sample from upper mould are taken our carefully. Then sample are left for curing for 14 days. If the testing is done on $15^{\circ}$-$30^{\circ}$ asperity sample then facing angle for the force is $30^{\circ}$.

**Fig 3.1:** Shows the Sample of direct shear test made up of Plaster of Paris.

## 3.2 CHARACTERIZATION OF MATERIAL USED FOR TESTING –

### 3.2.1 Determination of Specific Gravity [IS 2720 Part3]-

Specific gravity of Plaster of Paris can determined to IS 2720- part3, using Le-Chatelier flask. Firstly weight of clean flask with its stopper is taken ($W_1$) than sample weighing approximately 50 gm is placed into the flask such that it is half filled and again weighed with its stopper ($W_2$), polar liquid (kerosene) is added to POP in flask till it is about half filled and mixed thoroughly with glass rod to remove entrapped, more kerosene is added with continuous stirring till it flush with graduated mark. Outside surface of flask is dried and weighed ($W_3$). Empty the flask, clean it and refill it with clean kerosene flush it with graduated mark, wipe outside and weigh ($W_4$).

$$\text{Specific gravity} = \frac{W_1 - W_2}{(W_1 - W_2) - (W_3 - W_4)0.79} \tag{34}$$

Where, $W_1$ = Weight of empty flask

$W_2$ = Weight of flask + Plaster of Paris

$W_3$= Weight of flask + Plaster of Paris+ Kerosene

The specific gravity of Plaster of Paris obtained by this procedure is 2.08.

### 3.2.2 Determination of Initial and Final Setting Time of POP [IS 4031 (Part5): 1988]-

Determination of Initial and Final setting is very important for the molding in order to estimate the elapsed time between paste formation and initial hardening during the sample formation, as paste should be poured in the mould before initial setting and also sample should be taken out of the mould after final hardening.

Initial Setting time of cement is defined as the period elapsed between the time when the water is added to the cement and the time at which the needle of 1 $mm^2$ section fails to penetrate the test block to a depth of 5 $\pm$ 0.5 mm from the bottom of mould.

Final setting time of cement is defined as the period elapsed between the time when the water is added to the cement and the time at which the needle of area 1 $mm^2$ with 5 mm diameter attachment makes an impression on the test block, while the attachment fails to make an impression on the test block. Initial and final setting time of Plaster of Paris for 30%, 40% and 50% by weight is determined and shown below in table below:

**Table No.2:** Values of Initial/Final Setting Time of POP

| Water content % by Weight | Intial setting time (min) | Final setting Time (min) |
|---|---|---|
| 30 | 5.2 | 7.5 |
| 40 | 8.1 | 11.2 |
| 50 | 12.5 | 15.8 |

**3.2.3 UCS Test [ 7 Day And 14 Day] -** In Uniaxial Compressive Strength test the sample is subjected to uniaxial loading in which principal stress is acting only in longitudinal direction and no stress is acting along the other axis's .

Perpendicularity of the axis was not deviated by 0.001 radian and the specimen was tested after 7 day and 14 day. The prepared specimens (L=76 mm, D=38 mm) were put in between the two steel plates of the testing machine and load applied at the predetermined rate

along the axis of the sample till the sample fails. The deformation of the sample was measured with the help of separate dial gauge. During the test, load versus deformation readings were taken and a graph is plotted. When a brittle failure occurs, the proving ring dial indicates a definite maximum load which drops rapidly with the further increase of strain. The applied load at the point of failure was noted. The load is divided by the bearing surface of the specimen which gives the uniaxial compressive strength of the specimen.

Tests was conducted on the samples prepared by 30%, 40% and 50% water content (by weight) of Plaster of Paris for 7 days of curing and 14 day of curing (air dried curing) on the sample of 50% water content.

***The Experimental Stress-Strain Curve for POP obtained from UCS tests are shown below-***

**(I) For 30% w/c and 7 days of Curing-**

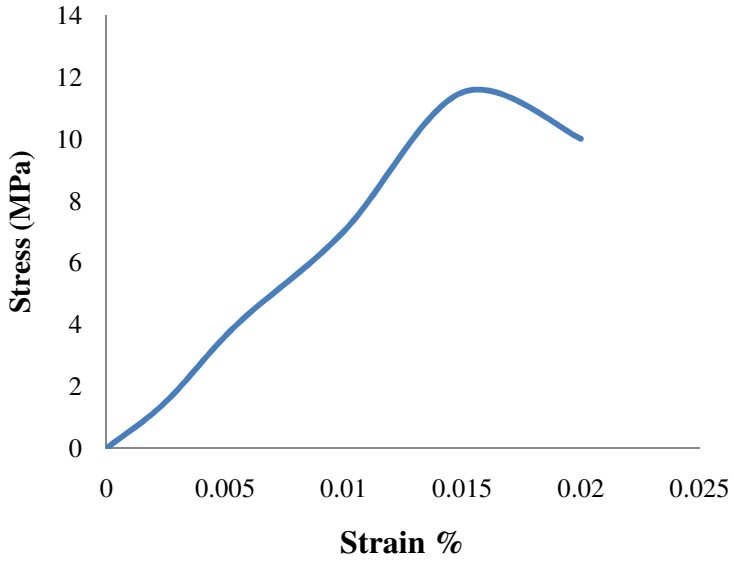


**Fig 3.2: Shows Stress-Strain Relation for 30% water content**

## (II) 40 % w/c and 7 days Curing-

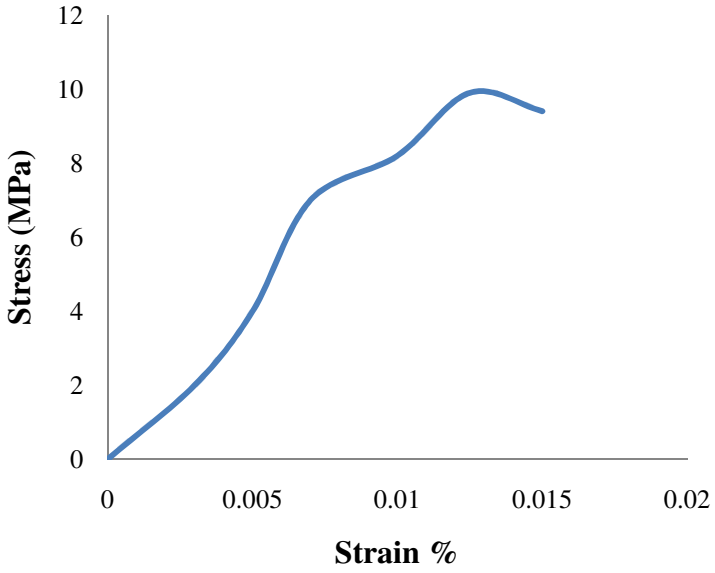


**Fig 3.3: Shows Stress-Strain Relation for 40% water content**

## (III) 50% w/c and 7 days of curing-

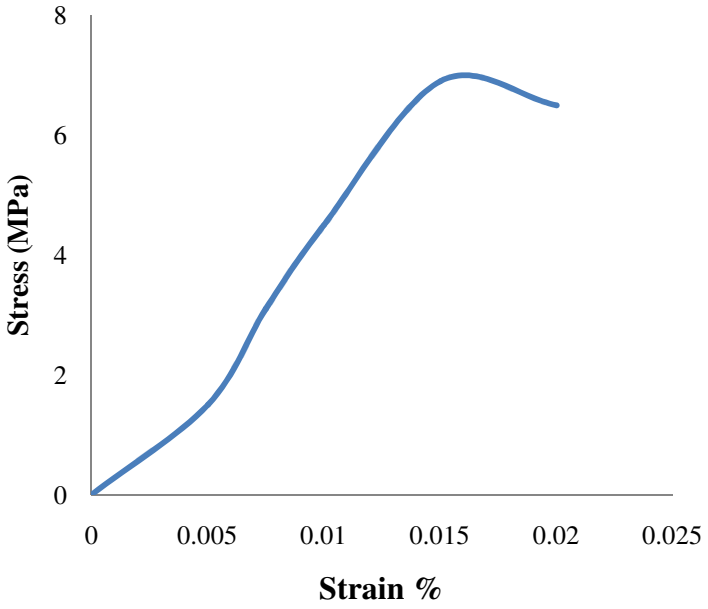


**Fig 3.4: Shows Stress-Strain Relation for 50% water content**

***Comparison of UCS values at different water content at 7 days of curing:-***

**Table No.3:** Values of UCS of POP

| w/c content | UCS values |
|---|---|
| 30% | 11.5 MPa |
| 40% | 10.0 MPa |
| 50% | 7.0 MPa |

### (IV) 50 % w/c and 14 days of curing-

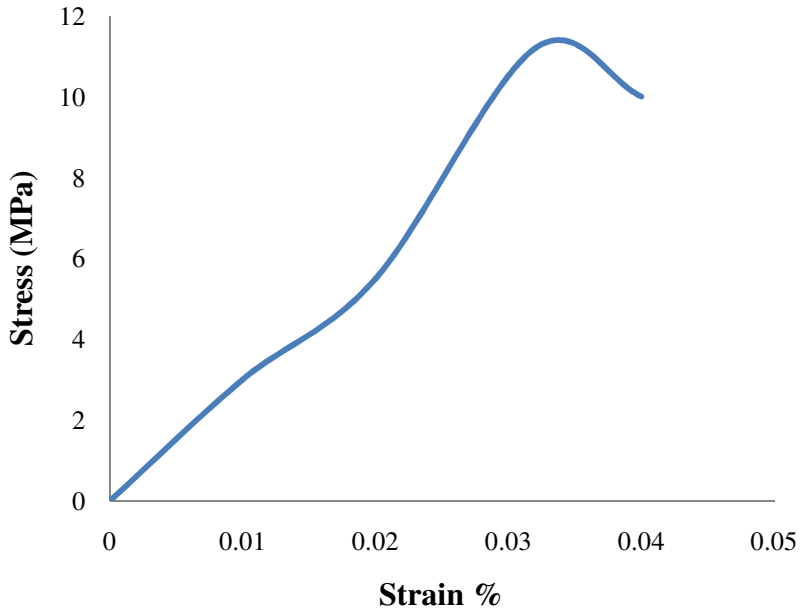


**Fig 3.5: Shows Stress-Strain Relation for 50% water content**

***Compressive strength for 50% water content after 14 day curing:*** Uniaxial Compressive Strength of Plaster of Paris for 50% water content after 14 curing is 11.2MPa.

## 3.3 DIRECT SHEAR TEST AT 14 DAYS [IS-2720 Part 13-1986] –

To achieve the aim of study of shear behaviour of soft rock joints, constant normal load (CNL) tests is conducted on artificial constructed gypsum plaster joints of identical surface profiles. The plaster joint (in two halves) has been cast within the twin-box assembly as explained earlier.

In direct shear test, bottom box can move only in the horizontal direction, while the top box can move only in the vertical direction during shearing. Test has been conducted on various

specimens of identical regular saw tooth profiles in the large shear apparatus under constant normal load. The test was conducted under normal stresses $\sigma_n$ = 0.05, 0.1, 0.2, 0.3, 0.4, 0.5 MPa.

During this test normal load is kept constant and shear resistance offered by joints due to interlocking, friction is measured. Test result, show the relationship between-

a) Dilation (vertical displacement/Horizontal displacement) vs. Shear (Horizontal) displacement

b) Shear Stress vs. Shear (Horizontal) displacement.

### 3.3.1 Standard of Materials-

Direct shear test is carried out with an apparatus consisting of a square divide into two halves. The specimen, contained in the box is subjected to a constant normal load, while an increasing horizontal force is applied to one of the sections of the shear box. This force causes a shear failure along junction between the box sections. The shear and normal force are measured with help of electronic unit attached with Conventional direct shear test machine. Rate of strain is adjusted by the speed of the horizontal force applied. The loading unit has V-strips on which the shear box housing rests. The size of specimen is fixed which is equal to 60 x 60 x 40 mm can be tested. Normal and shear displacement are measured with the help of linear variable differential transducers (LVDT's) having range of 20 mm, the sensitivities of LVDT's are 0.025 mm for shear displacement and 0.0025 mm for normal displacement. Rate of strain can be varied from 0.002 mm/min to 1.25 mm/min. Apparatus consist of digital indicator and for display consist of micro-controller multi line VFD display.

### 3.3.2 Preparation of Sample –

The preparation of sample for direct shear test is difficult task .Various moulds were prepared for the preparation of sample but many of them were numerous disadvantages, so constant preparation of mould leads to the success in preparation of the sample. Various moulds are prepared for the preparation of samples. Sample of $15^{\circ}$-$45^{\circ}$ asperity sample are same as that of the $45^{\circ}$-$15^{\circ}$, the difference is only the orientation of the sample during testing. The mould and sample of different asperity angle is shown:

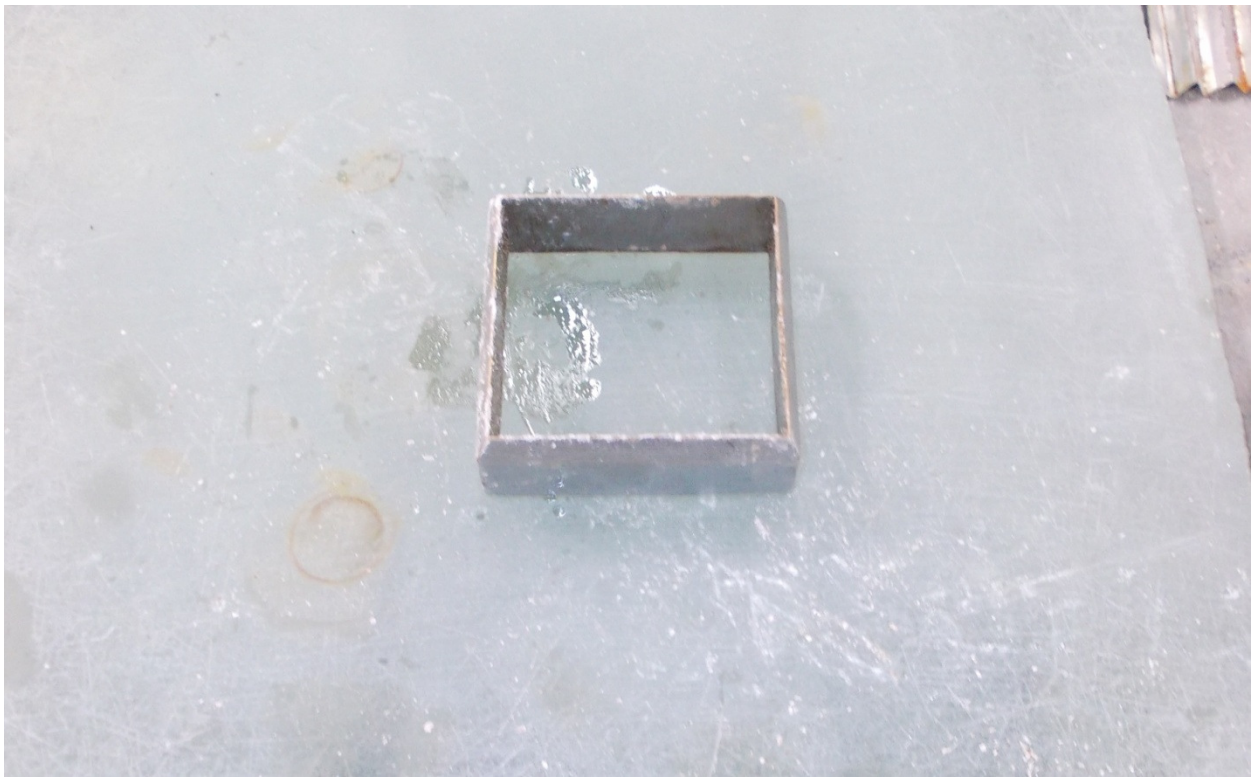

**Fig 3.6:** Shows the mould of size 60 x 60 mm used for preparation of sample

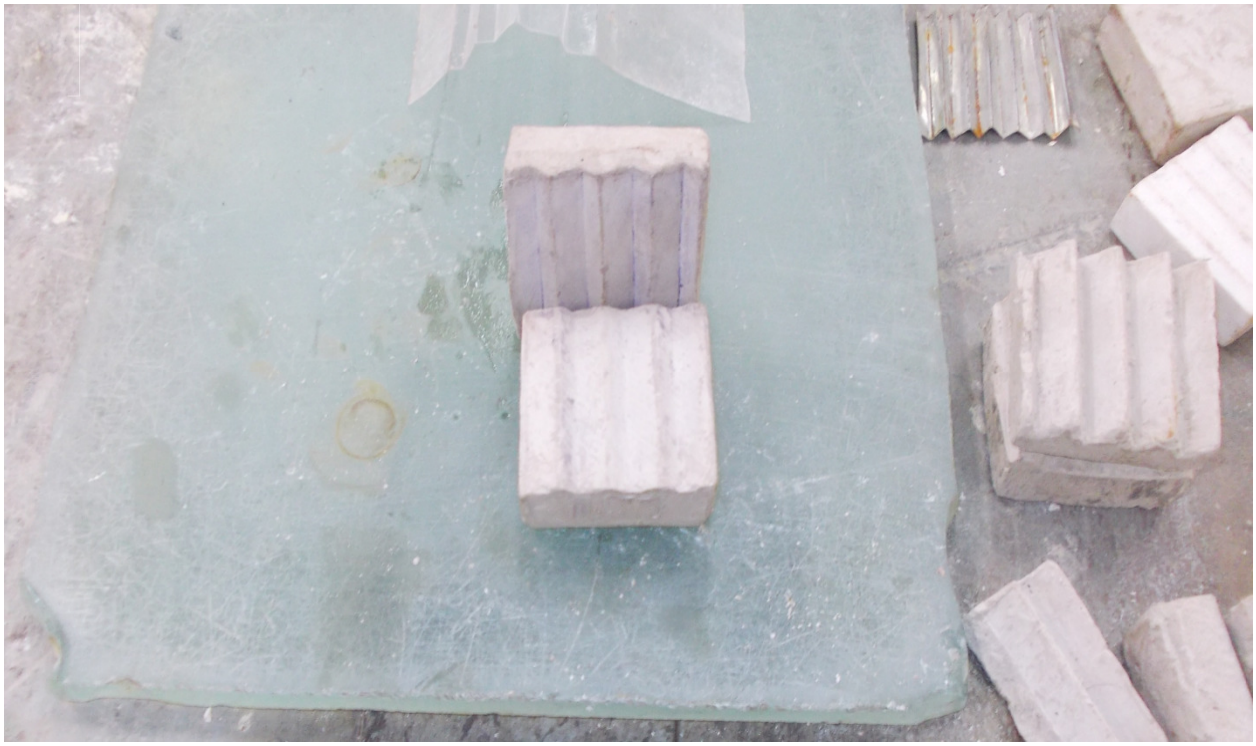

**Fig 3.7:** Shows the direct shear test sample of $15^{\circ}$-$30^{\circ}$ asperity

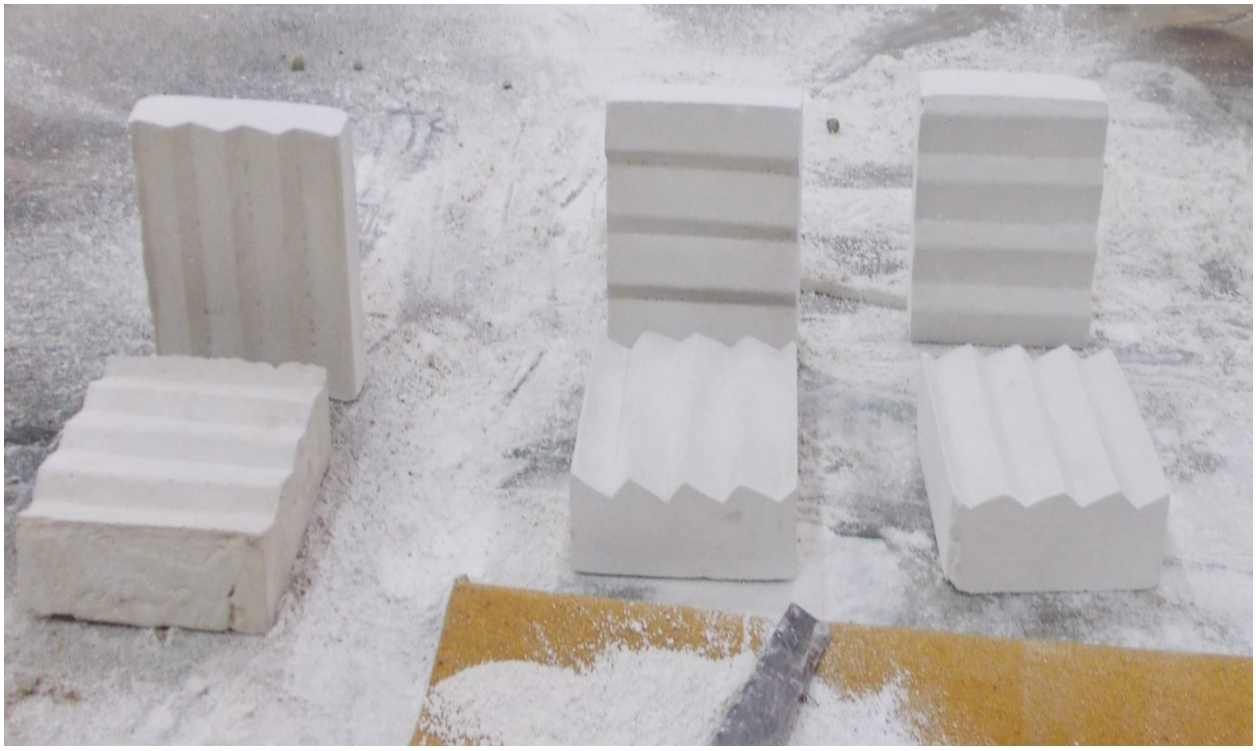

**Fig 3.8:** Shows the direct shear test sample of 15°-45° asperity

### 3.3.3 Results of Direct Shear Tests –

Shear test was performed at five different normal stresses under constant normal load condition (CNL). The normal stresses are 0.05 MPa. 0.1 MPa, 0.2 MPa, 0.3 MPa, 0.4 MPa and 0.5 MPa and samples prepared with asperity angle of 15°-30°, 15°-45° and 45°-15° are tested.

### 3.3.3.1 For 15°-30° asperity sample-

Direct shear test for sample containing saw tooth joints at an inclination i.e. at an asperity angle of 15°- 30° under CNL condition at different normal stresses after 14 days of air curing are tested. Figures shows the graph obtained after shear test between shear stress or resistance offered by the joint vs. Shear Displacement and Dilation vs. shear displacement at $\sigma_n$ = 0.05 MPa,0.1 MPa,0.2 MPa,0.3 MPa, 0.4 MPa and 0.5 MPa respectively.

## (I) $\sigma_n$= 0.05 MPa

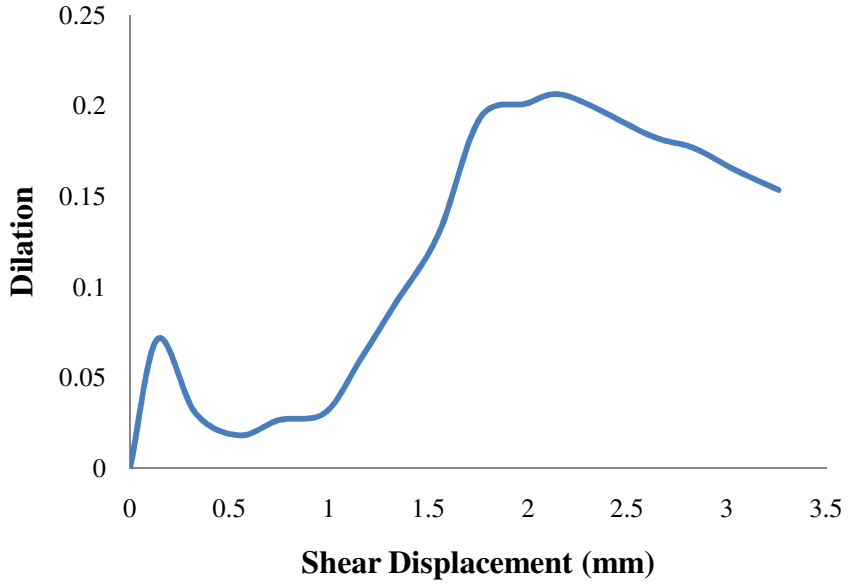


**a) Dilation vs. Shear Displacement**

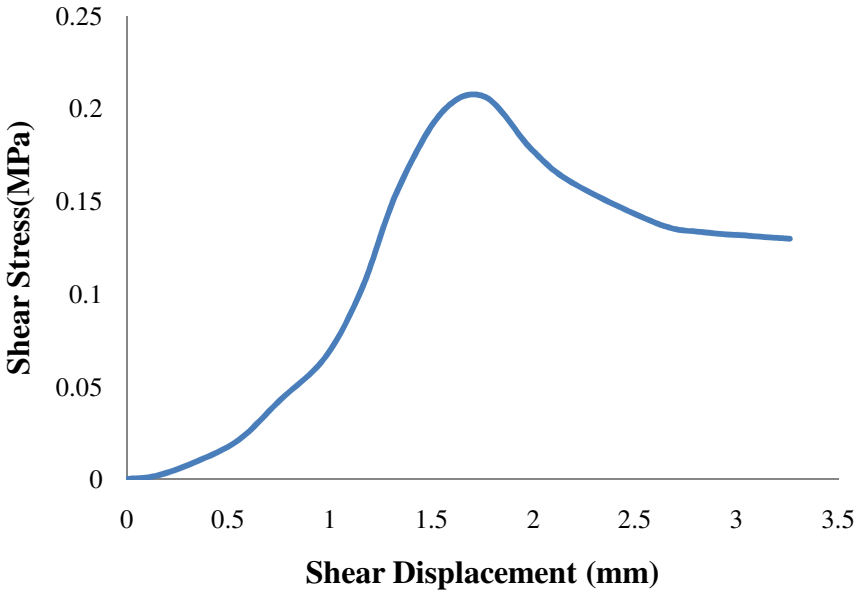


**b) Shear stress vs. Shear Displacement**

**Fig 3.9: a) & b) SHOWS SHEAR AND DILATION BEHAVIOUR OF 15°-30° ASPERITY SAMPLE UNDER $\sigma_n$= 0.05 MPa**

## II) $\sigma_n$= 0.1 MPa

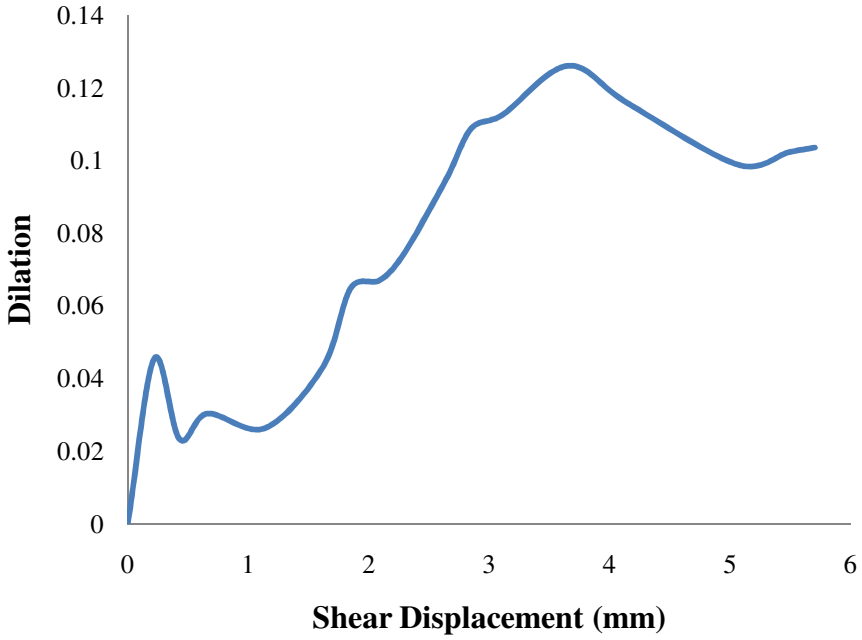


**a ) Dilation vs. Shear Displacement**

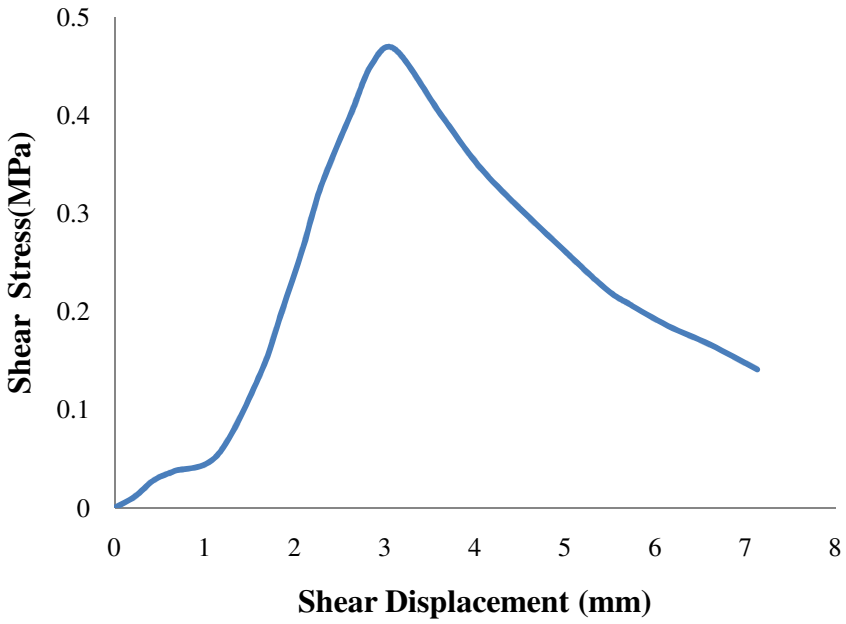


**b) Shear Stress vs. Shear Displacement**

**Fig 3.10: a) & b): SHEAR AND DILATION BEHAVIOUR OF 15°-30° ASPERITY SAMPLE UNDER $\sigma_n$ = 0.1MPa**

## III) $\sigma_n$= 0.2 MPa

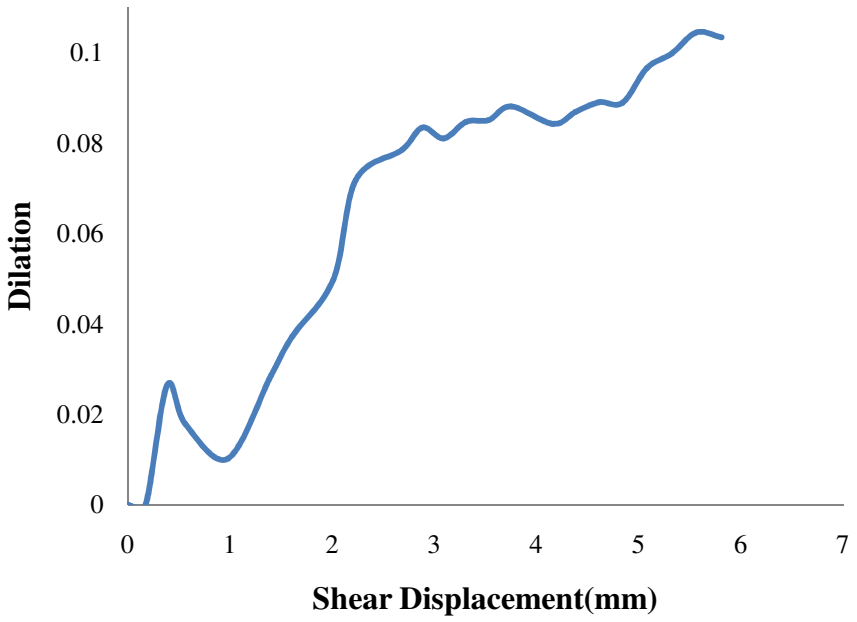


**a) Dilation vs. Shear Displacement**

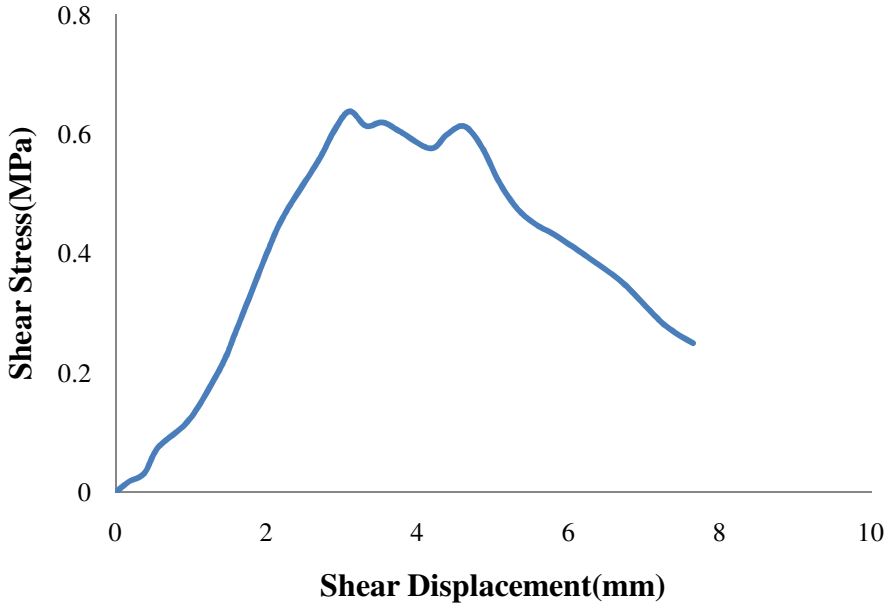


**b) Shear stress vs. Shear Displacement**

**Fig 3.11 a) & b): SHEAR AND DILATION BEHAVIOUR OF 15°-30° ASPERITY SAMPLE UNDER $\sigma_n$= 0.2 MPa**

## IV) $\sigma_n$= 0.3 MPa

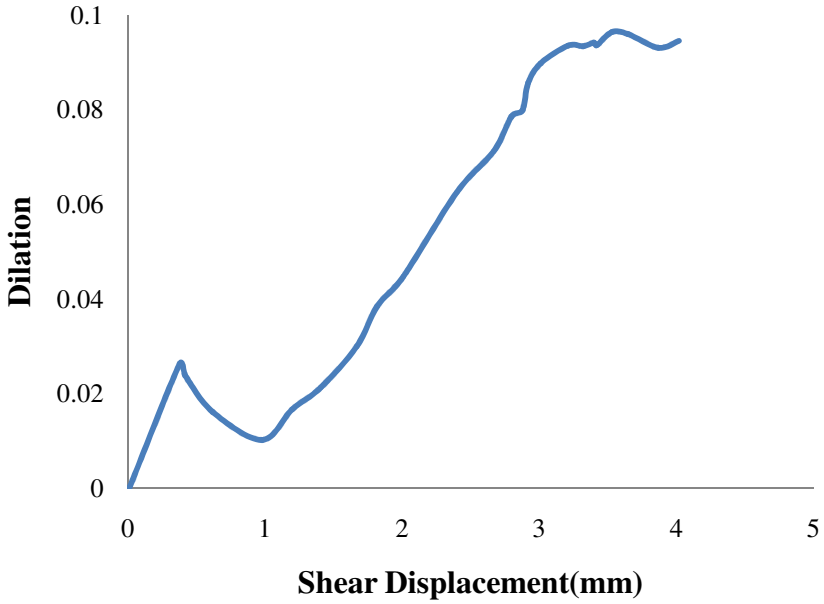


**a) Dilation vs. Shear Displacement**

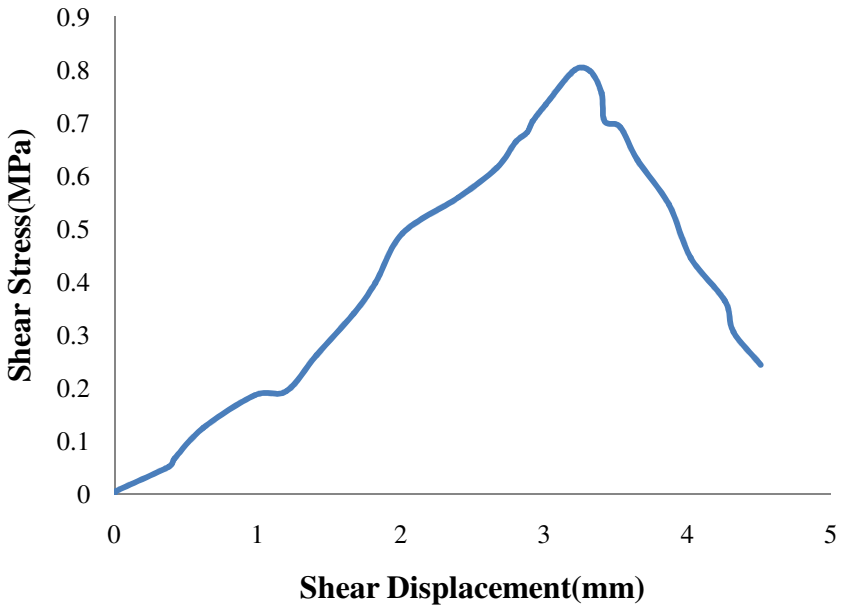


**b) Shear stress vs. Shear Displacement**

**Fig 3.12 a) & b): SHEAR AND DILATION BEHAVIOUR OF 15°-30° ASPERITY SAMPLE UNDER $\sigma_n$ = 0.3 MPa**

## V) $\sigma_n$ = 0.4 MPa

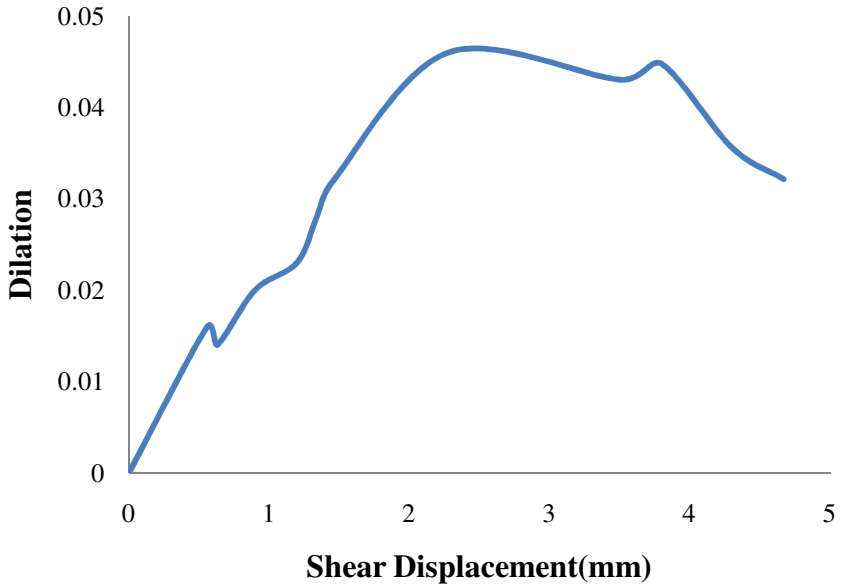


**a) Dilation vs. Shear Displacement**

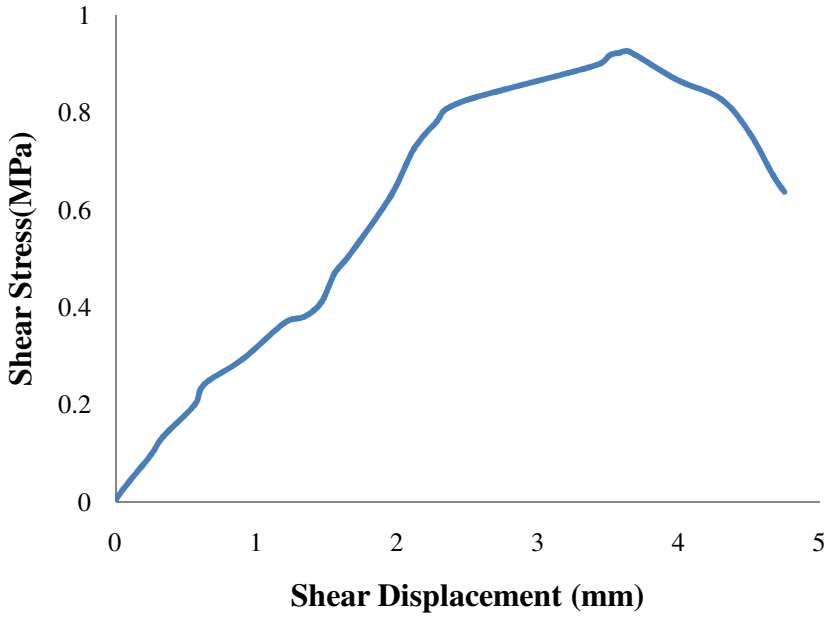


**b) Shear Stress vs. Shear Displacement**

**Fig 3.13 a) & b): SHEAR AND DILATION BEHAVIOUR OF 15°-30° ASPERITY SAMPLE UNDER $\sigma_n$ = 0.4 MPa**

## VI) $\sigma_n$= 0.5 MPa

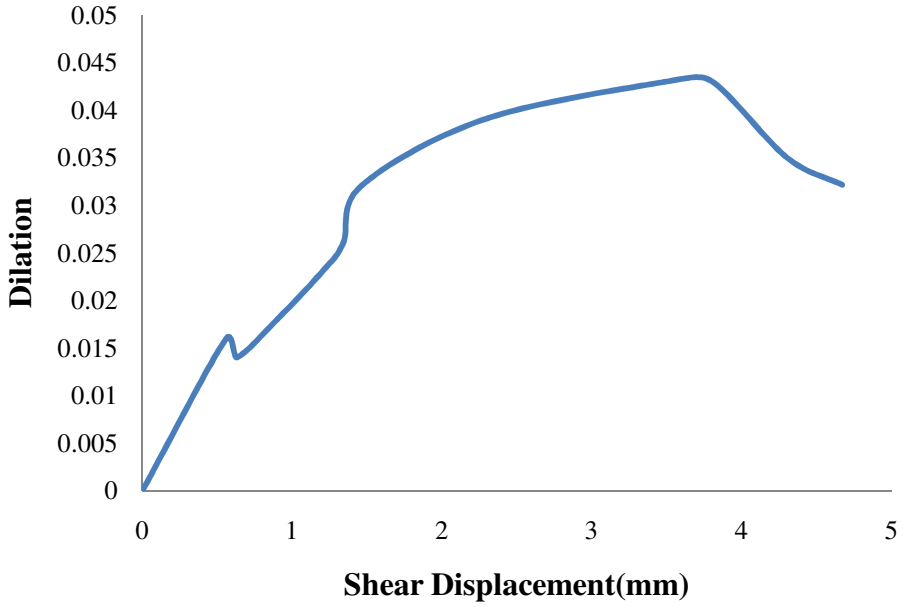


**a) Dilation vs. Shear Displacement**

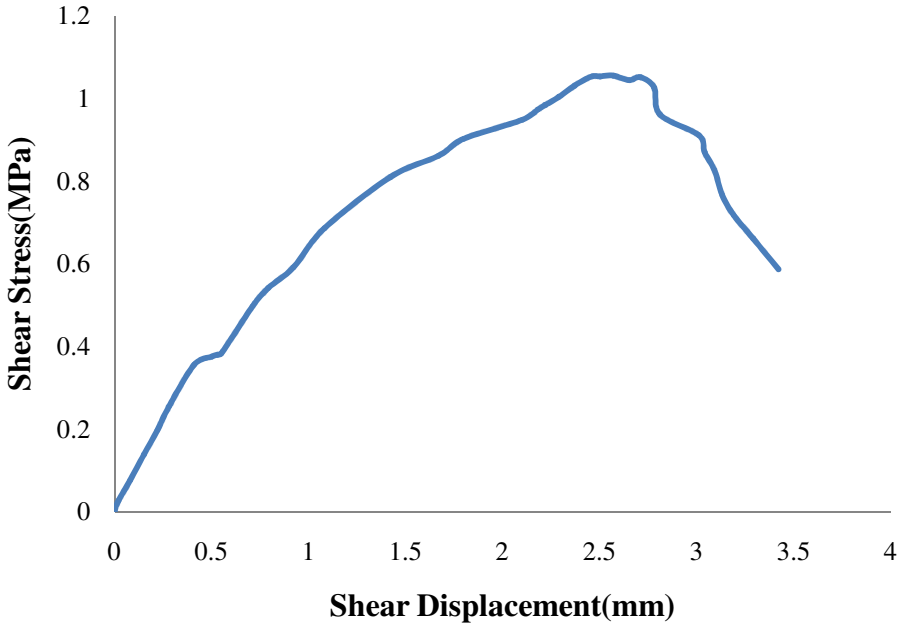


**b) Shear Stress vs. Shear Displacement**

**Fig 3.14 a) & b): SHEAR AND DILATION BEHAVIOUR OF 15°-30° ASPERITY SAMPLE UNDER $\sigma_n$ = 0.5 MPa**

### 3.3.3.2 For 15°-45° asperity sample-

Direct shear test for sample containing saw tooth joints at an inclination i.e. at an asperity angle of 15°-45° under CNL condition at different normal stresses after 14 days of air curing are tested. Figures shows the graph obtained after shear test between shear stress or resistance offered by the joint vs. shear displacement and dilation vs. shear displacement at $\sigma_n$ = 0.05 MPa, 0.1 MPa, 0.2 MPa, 0.3 MPa, 0.4 MPa and 0.5 MPa respectively.

## (I) $\sigma_n$ = 0.05 MPa

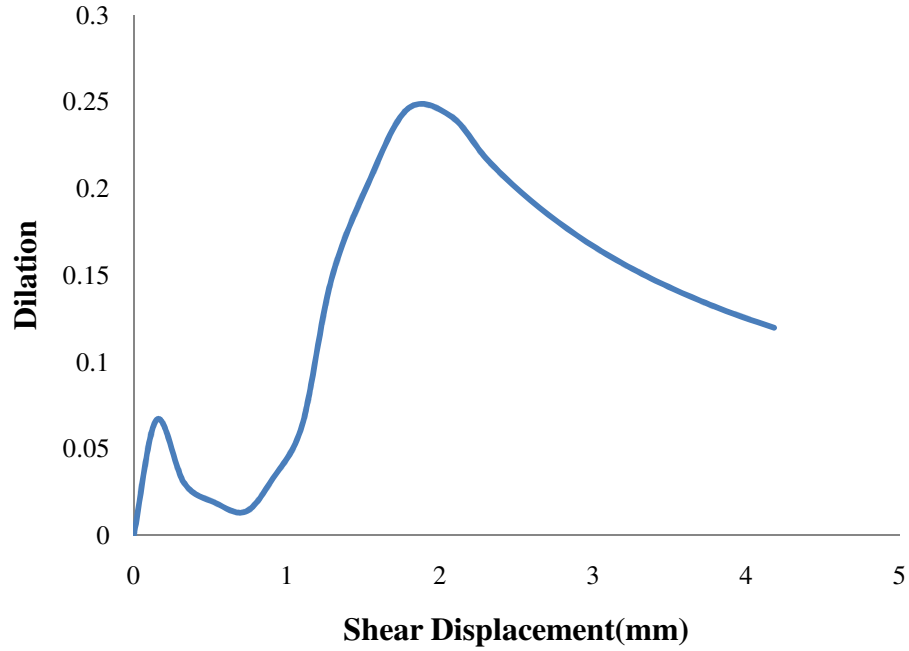


**a) Dilation vs. Shear Displacement**

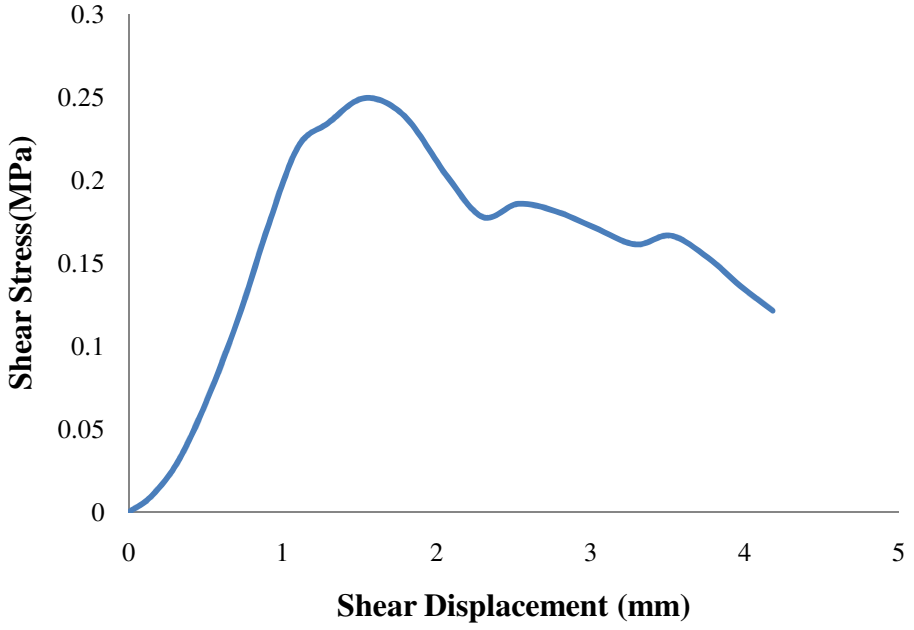


**b) Shear Stress vs. Shear Displacement**

**Fig 3.15 a) & b): SHEAR AND DILATION BEHAVIOUR OF 15°-45° ASPERITY SAMPLE UNDER $\sigma_n$= 0.05 MPa**

**(II) $\sigma_n$= 0.1 MPa**

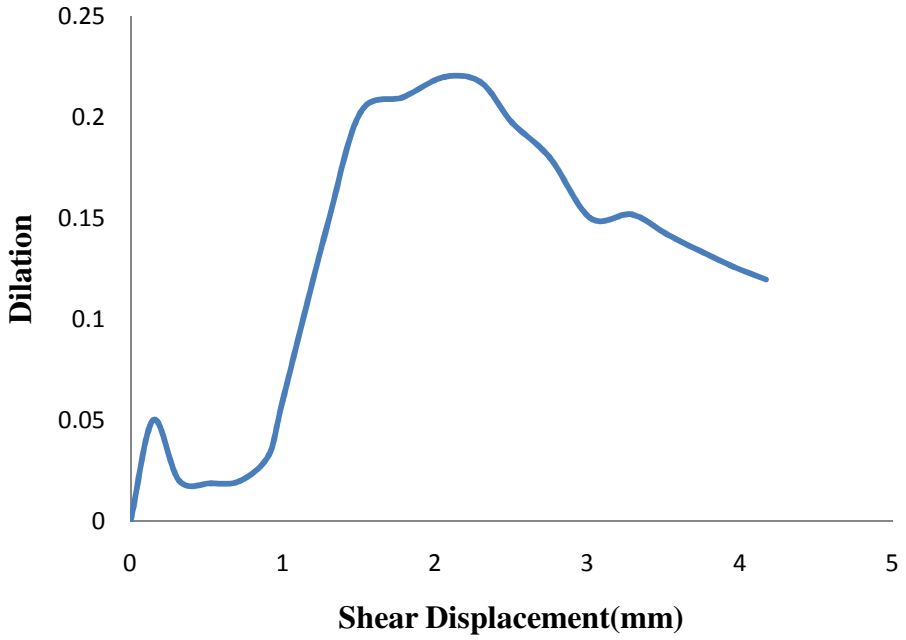


**a) Dilation vs. Shear Displacement**

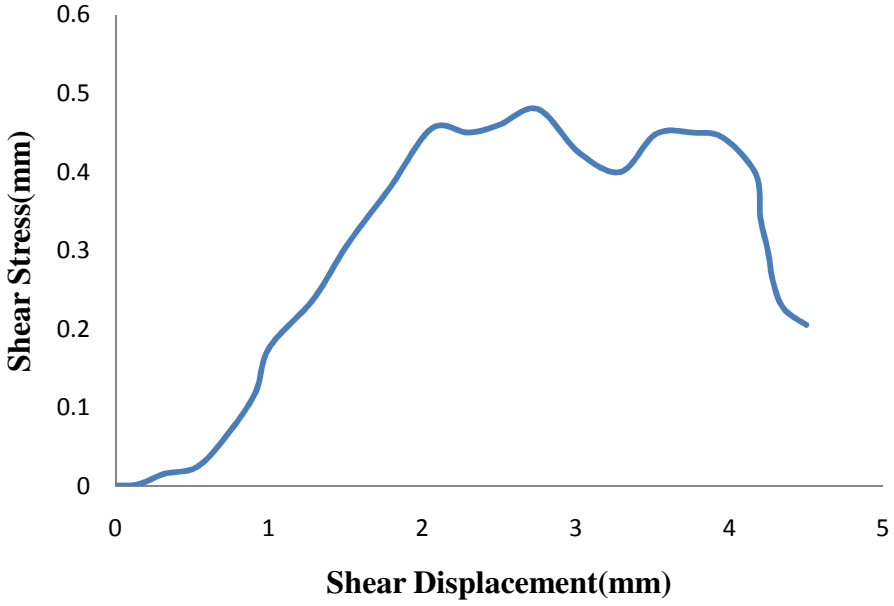


**b) Shear Stress vs. Shear Displacement**

**Fig 3.16 a) & b): SHEAR AND DILATION BEHAVIOUR OF 15°-45° ASPERITY SAMPLE UNDER $\sigma_n$= 0.1 MPa**

## (III) $\sigma_n$= 0.2 MPa

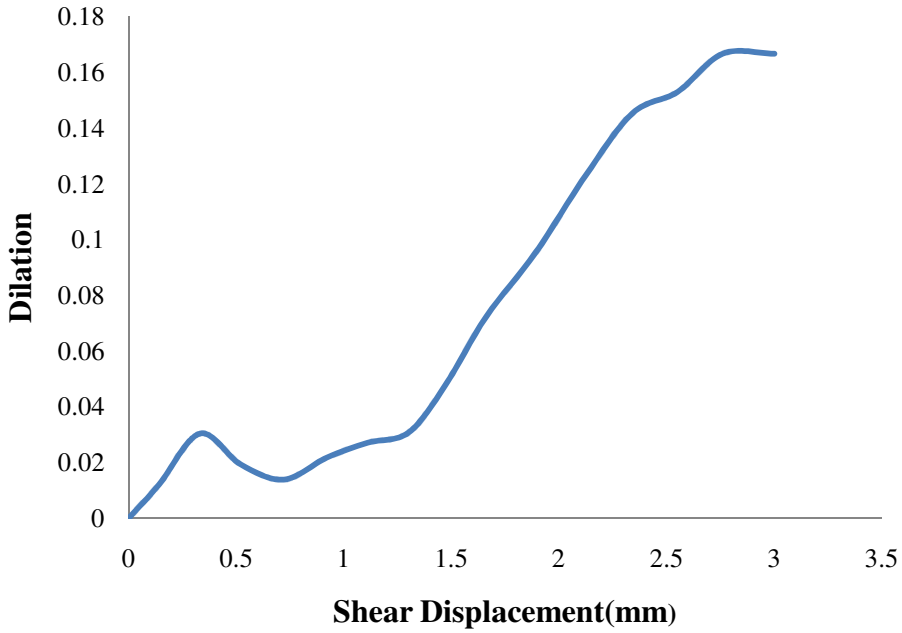


**a) Dilation vs. Shear Displacement**

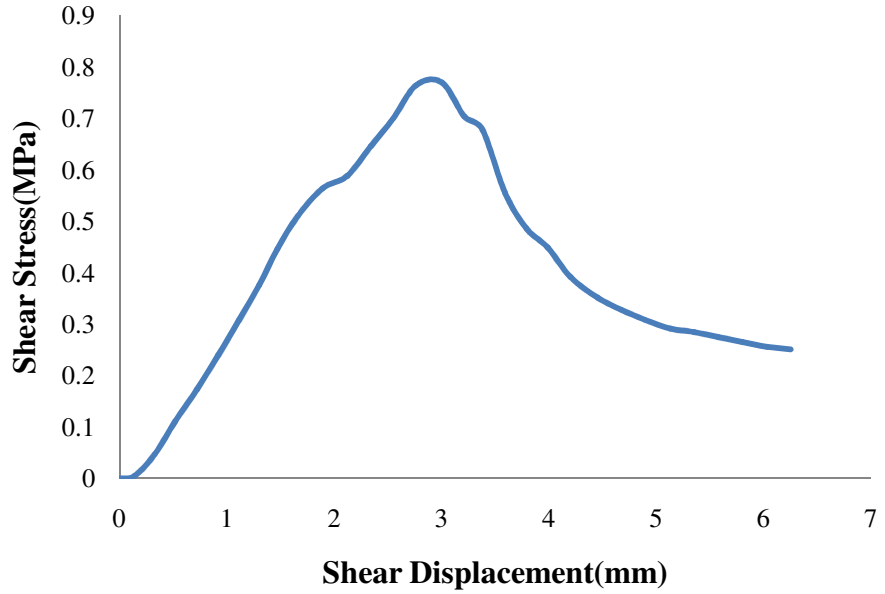


**b) Shear Stress vs. Shear Displacement**

**Fig 3.17 a) & b): SHEAR AND DILATION BEHAVIOUR OF 15°-45° ASPERITY SAMPLE UNDER $\sigma_n$= 0.2 MPa**

## IV) $\sigma_n$= 0.3 MPa

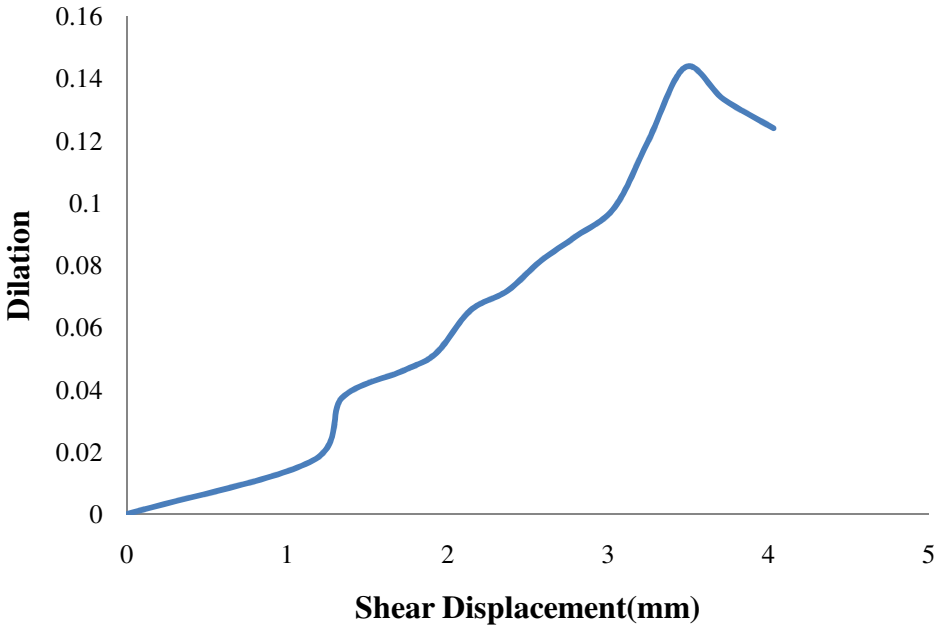


**a) Dilation vs. Shear Displacement**

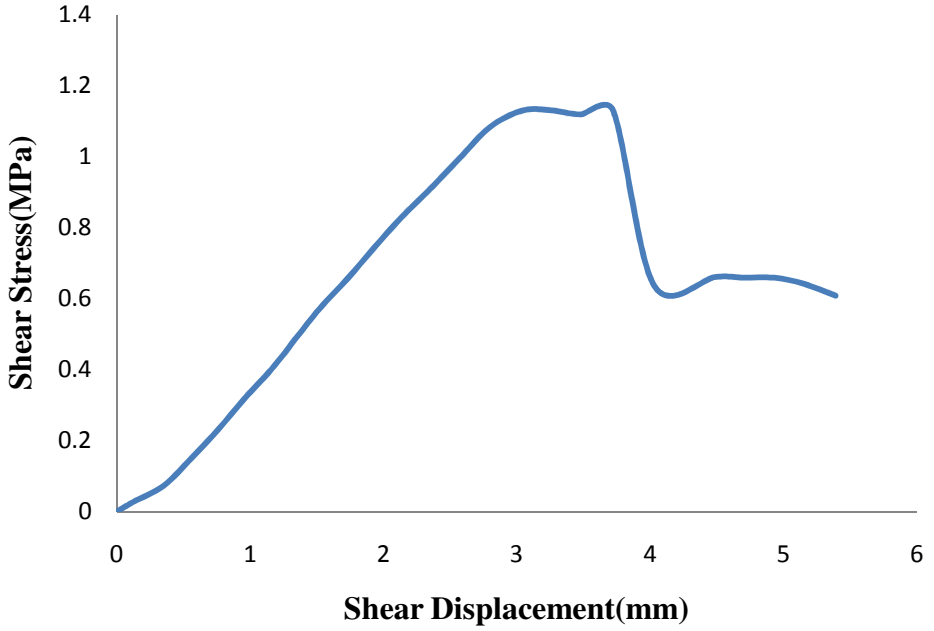


**b) Shear Stress vs. Shear Displacement**

**Fig 3.18 a) & b): SHEAR AND DILATION BEHAVIOUR OF 15°-45° ASPERITY SAMPLE UNDER $\sigma_n$= 0.3 MPa**

**V) $\sigma_n$= 0.4 MPa**

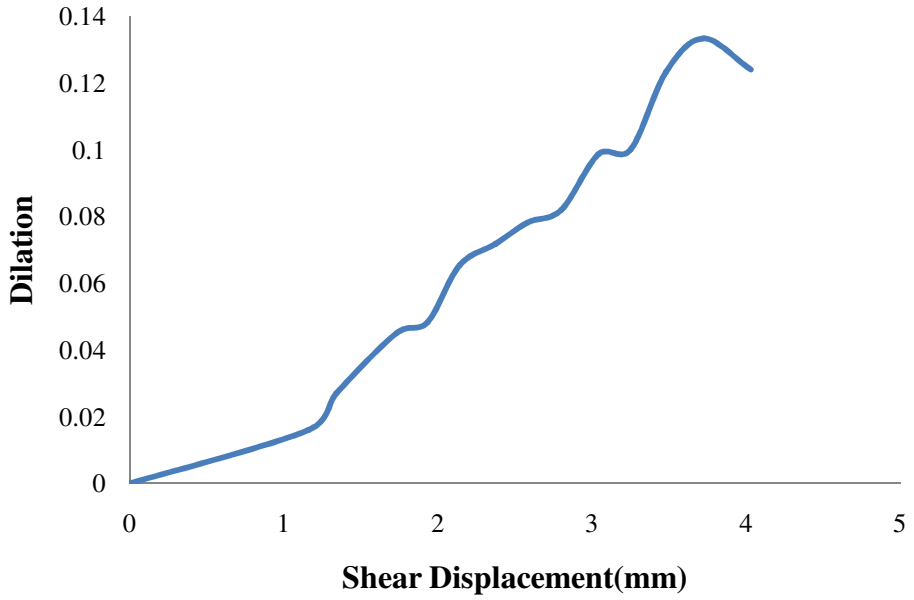


**a) Dilation vs. Shear Displacement**

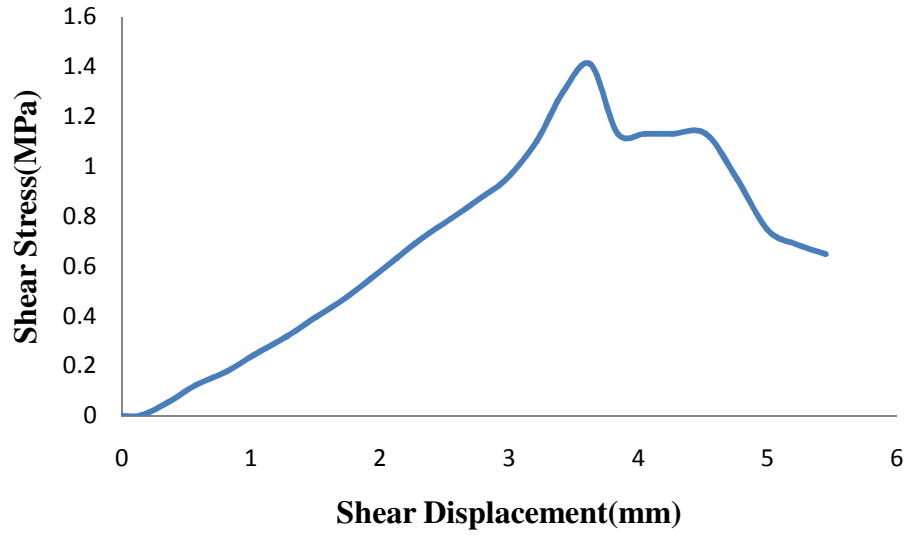


**b) Shear stress vs. Shear Displacement**

**Fig 3.19 a) & b): SHEAR AND DILATION BEHAVIOUR FOR 15°-45° ASPERITY SAMPLE UNDER $\sigma_n$ = 0.4 MPa**

## VI) $\sigma_n$= 0.5 MPa

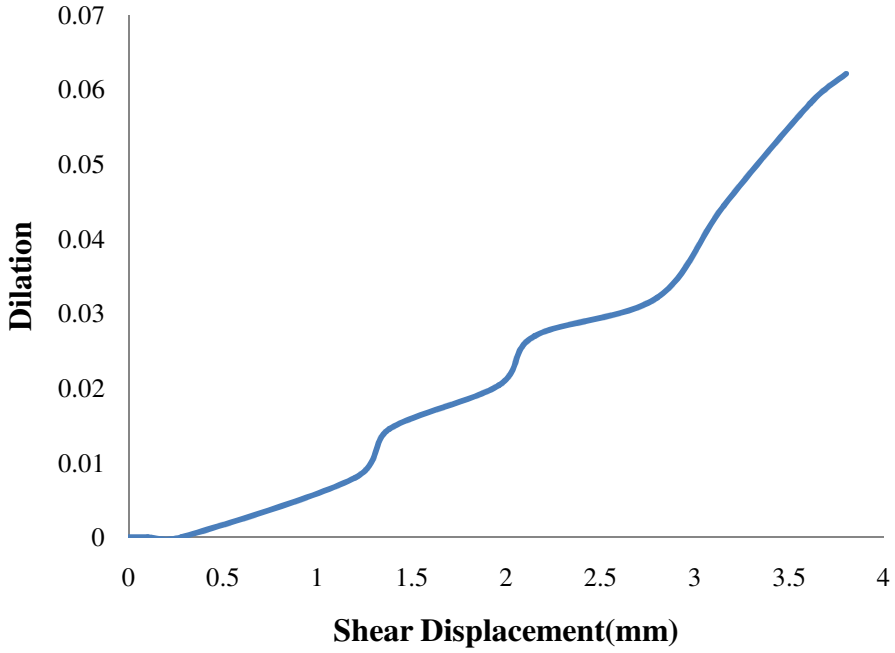


**a) Dilation vs. Shear Displacement**

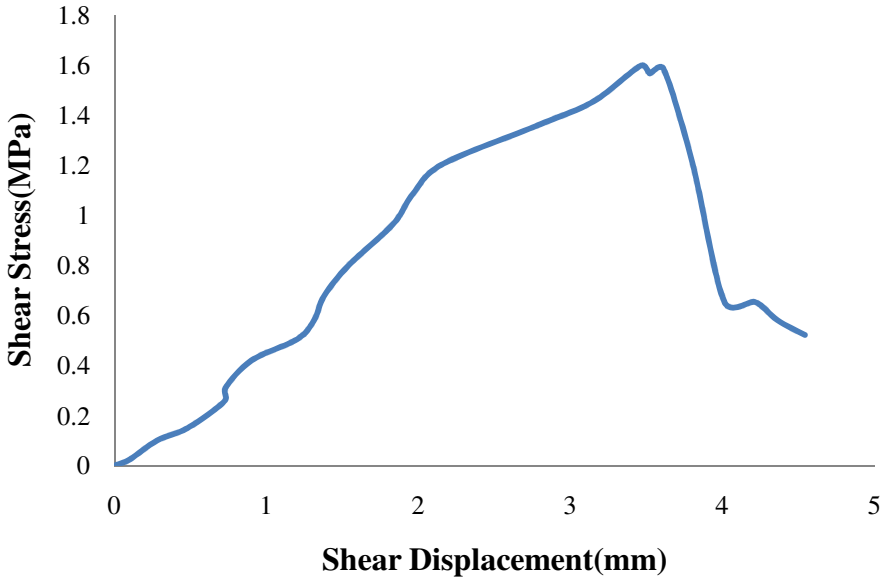


**b) Shear Stress vs. Shear Displacement**

**Fig 3.20 a) & b): SHEAR AND DILATION BEHAVIOUR OF 15°-45° ASPERITY SAMPLE UNDER $\sigma_n$ = 0.5 MPa**

### 3.3.3.3 For $45^{\circ}$-$15^{\circ}$ Asperity Angle:

Direct shear test for sample containing saw tooth joints at an inclination i.e. at an asperity angle of $45^{\circ}$-$15^{\circ}$ under CNL condition at different normal stresses after 14 days of air curing are tested. Figures shows the graph obtained after shear test between shear stress or resistance offered by the joint vs. Shear Displacement and Dilation vs. shear displacement at $\sigma_n$ = 0.05 MPa, 0.1 MPa, 0.2 MPa, 0.3 MPa, 0.4 MPa and 0.5 MPa respectively.

**(I) $\sigma_n$ = 0.05 MPa**

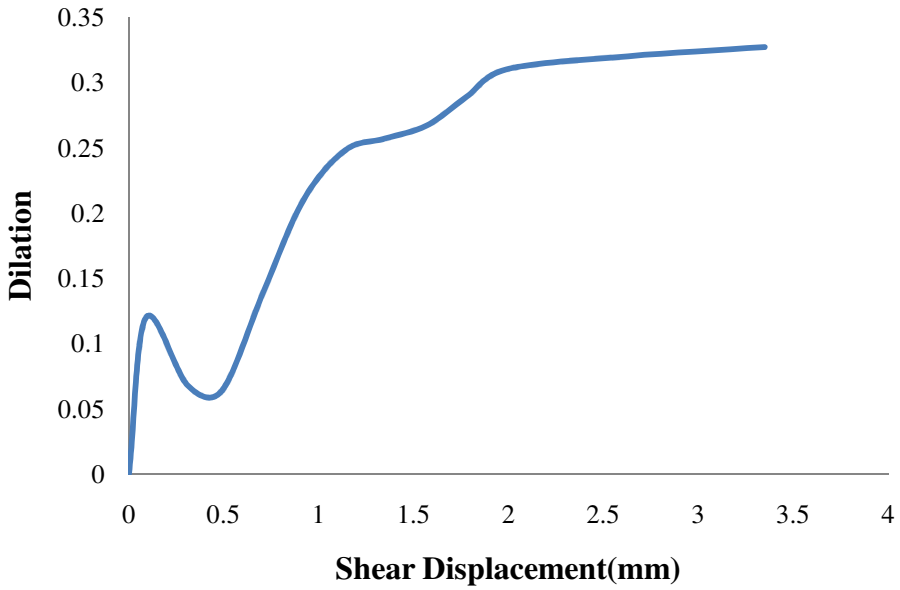


**a) Dilation vs. Shear Displacement**

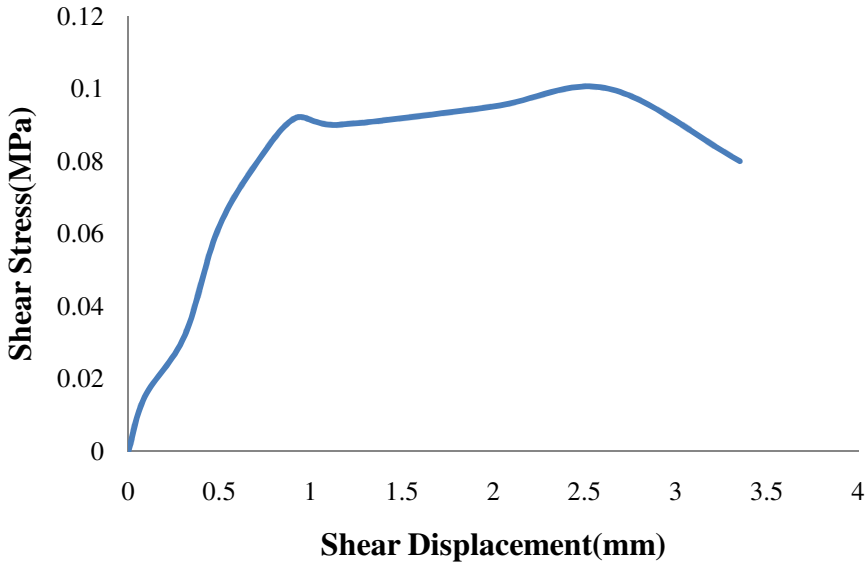


**b) Shear Stress vs. Shear Displacement**

**Fig 3.21 a) & b): SHEAR AND DILATION BEHAVIOUR OF 45°-15° ASPERITY SAMPLE UNDER $\sigma_n$= 0.05 MPa**

**(III) $\sigma_n$= 0.1 MPa-**

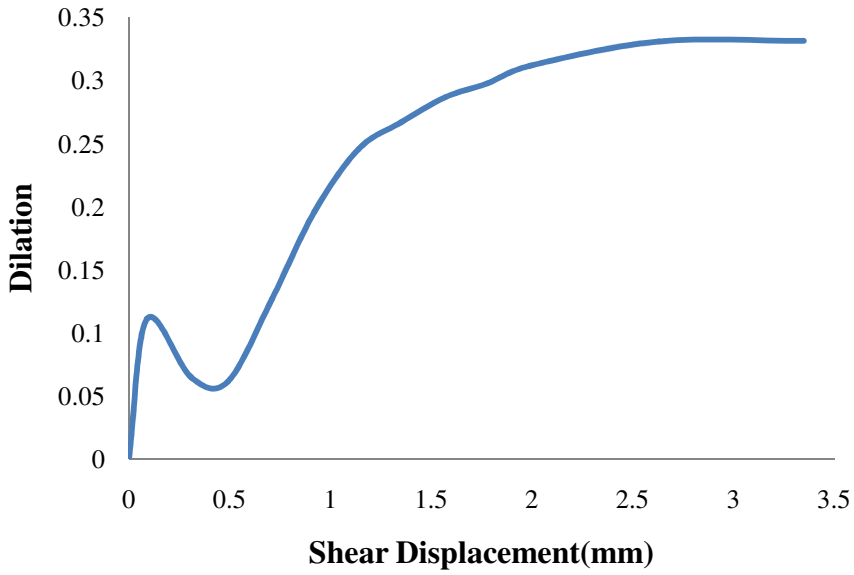


**a) Dilation vs. Shear Displacement**

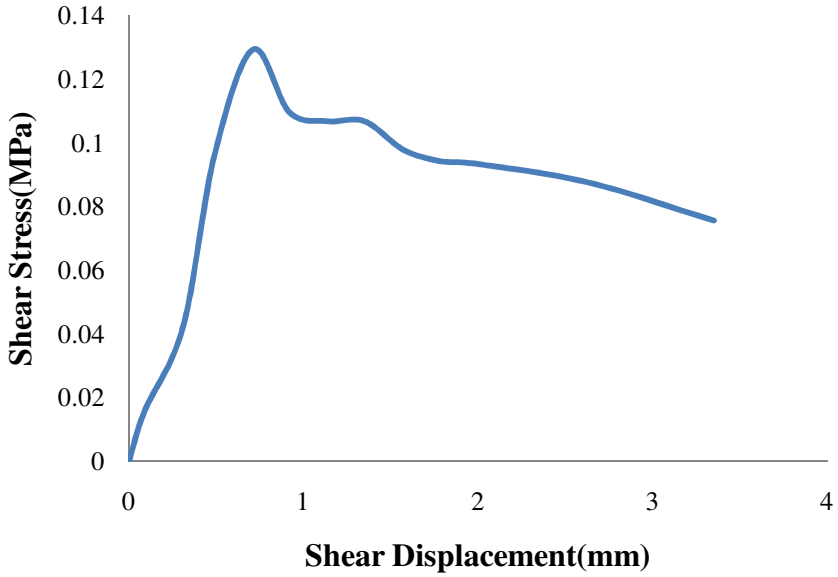


**b) Shear Stress vs. Shear Displacement**

**Fig 3.22 a) & b): SHEAR AND DILATION BEHAVIOUR OF 45°-15° ASPERITY SAMPLE UNDER $\sigma_n$= 0.1 MPa**

**(IV) $\sigma_n$ = 0.2 MPa**

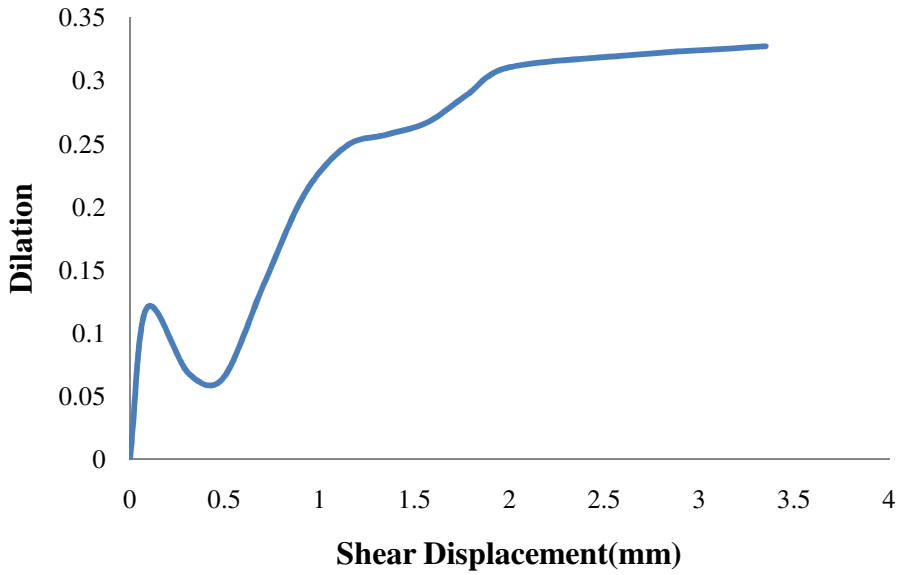


**a) Dilation vs. Shear Displacement**

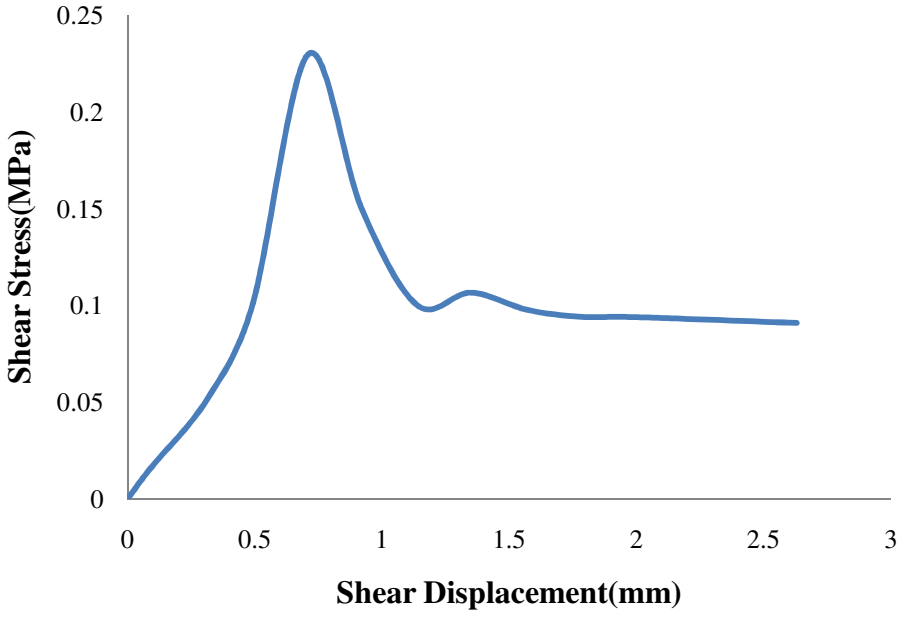


**b) Shear Stress vs. Shear Displacement**

**Fig 3.23 a) & b): SHEAR AND DILATION BEHAVIOUR OF 45°-15° ASPERITY SAMPLE UNDER $\sigma_n$= 0.2 MPa**

**(V) $\sigma_n$ = 0.3 MPa**

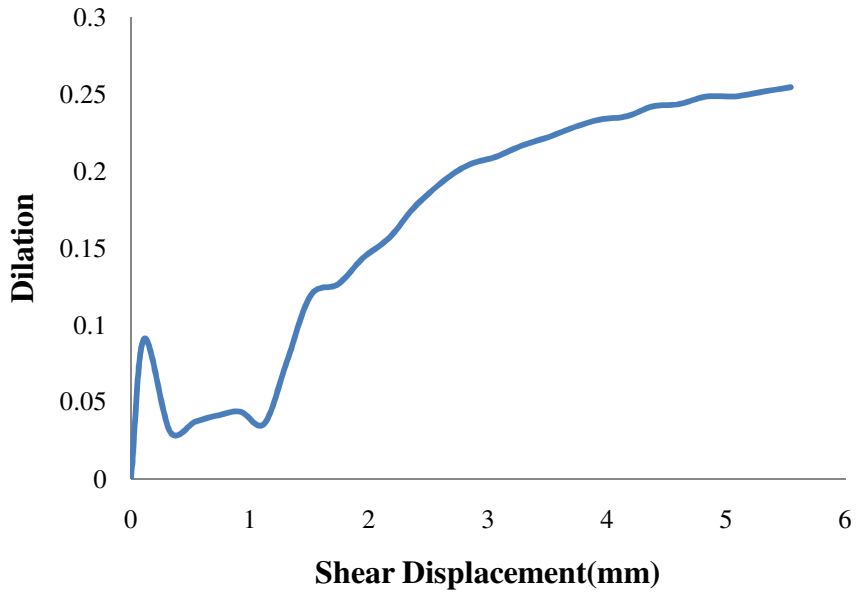


**a) Dilation vs. Shear Displacement**

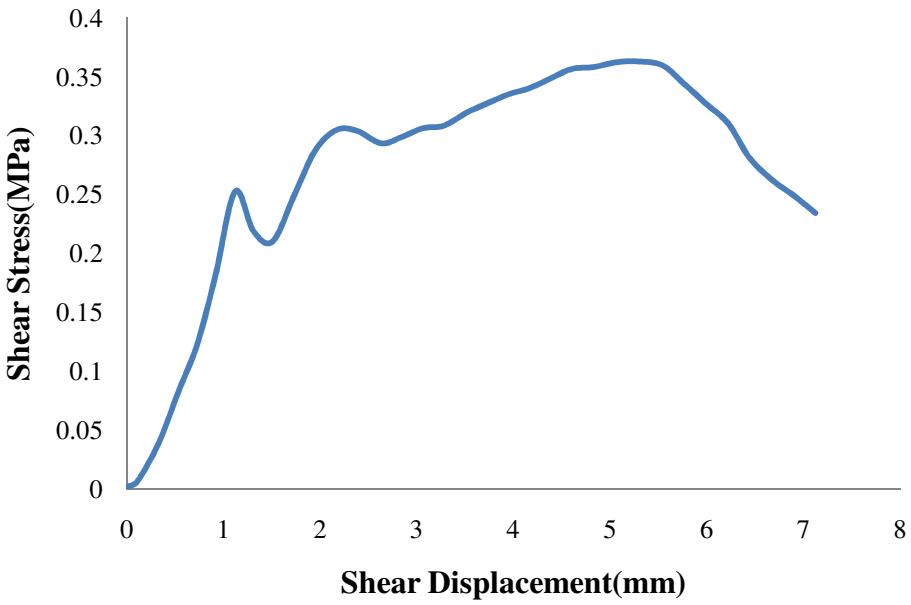


**b) Shear Stress vs. Shear Displacement**

**Fig 3.24 a) & b): SHEAR AND DILATION BEHAVIOUR OF 45°-15° ASPERITY UNDER $\sigma_n$= 0.3 MPa**

**(V) $\sigma_n$ = 0.4 MPa**

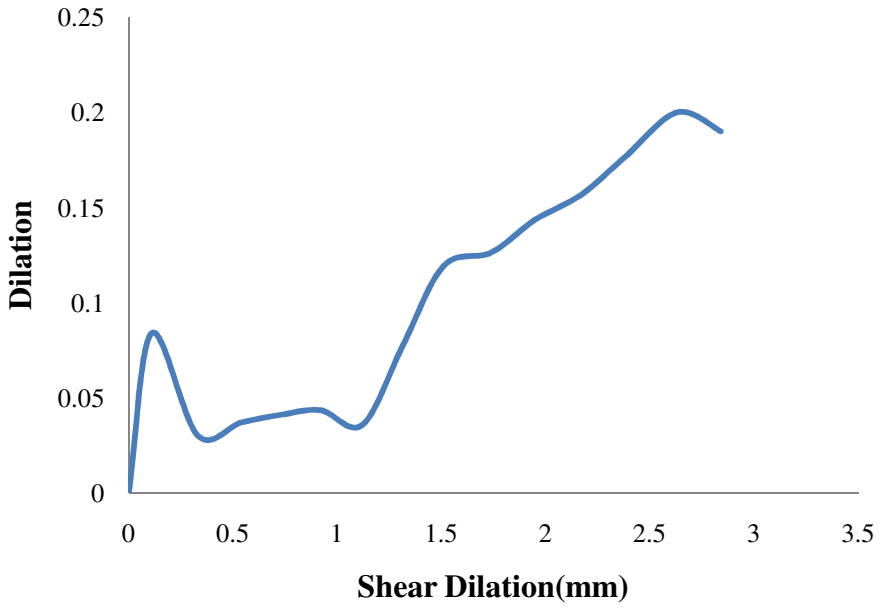


**a) Dilation vs. Shear Displacement**

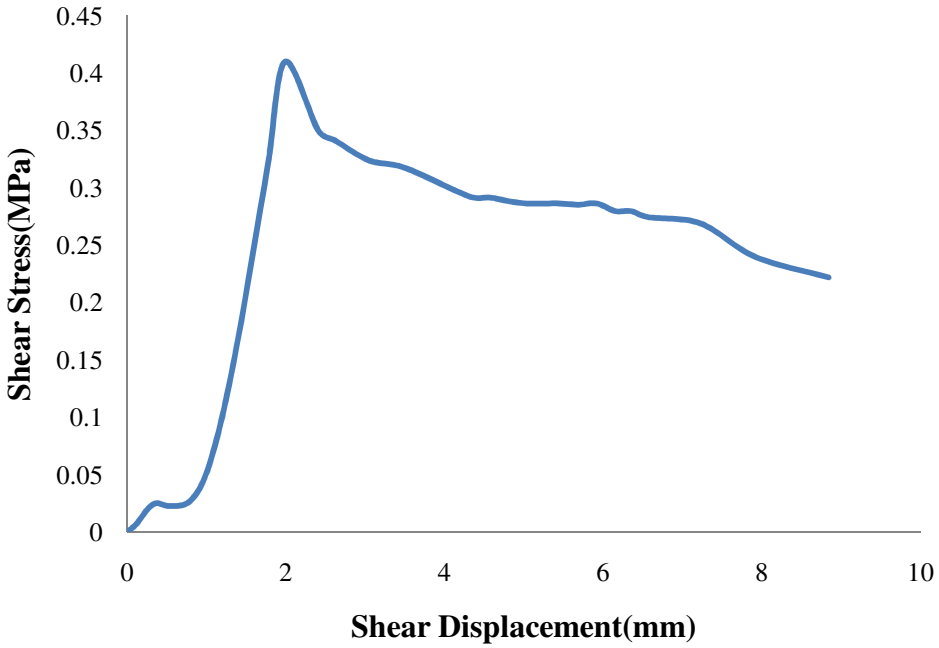


**b) Shear stress vs. Shear Displacement**

**Fig 3.25 a) & b): SHEAR AND DILATION BEHAVIOUR OF 45°-15° ASPERITY SAMPLE UNDER $\sigma_n$ = 0.4 MPa**

**(VI) $\sigma_n$ = 0.5MPa**

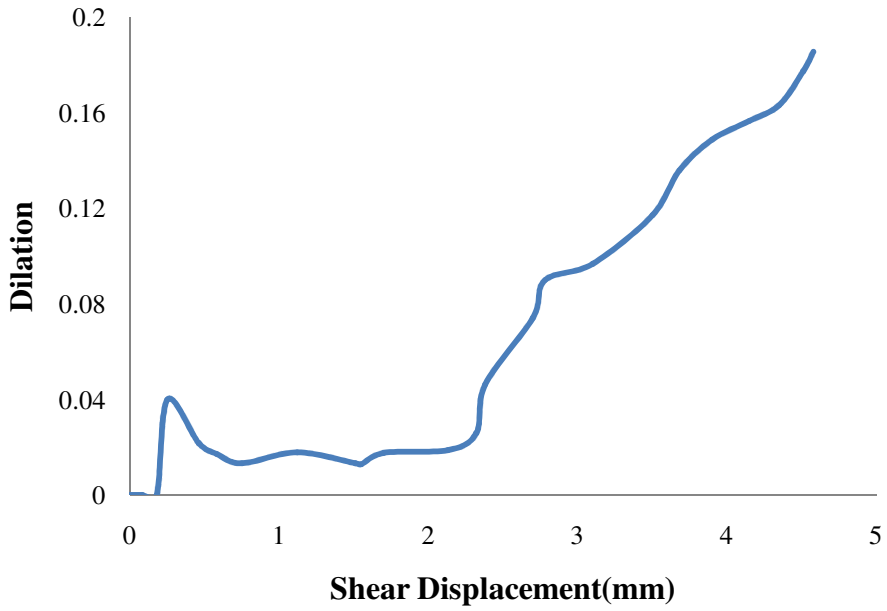


**a) Dilation vs. Shear Displacement**

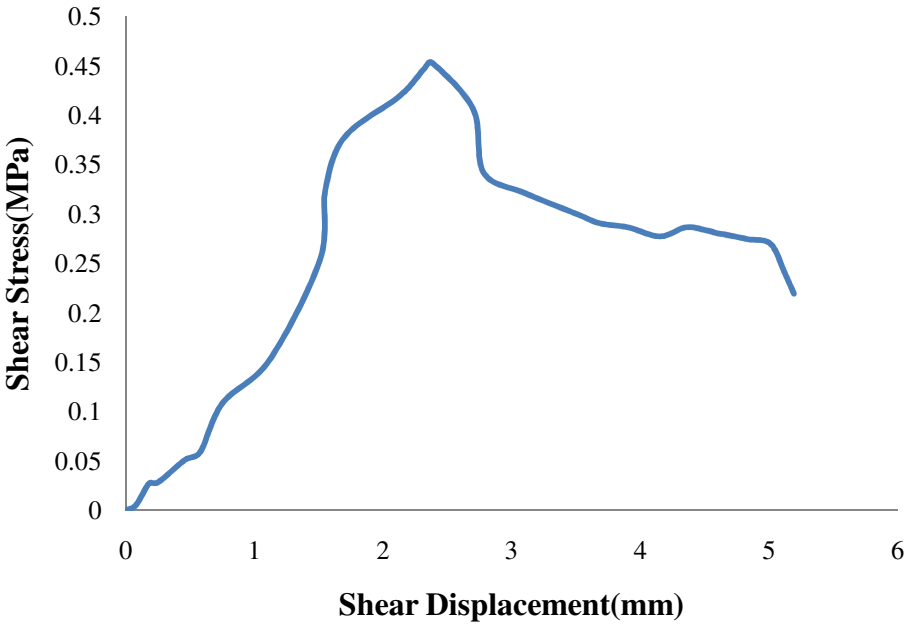


**b) Shear stress vs. Shear Displacement**

**Fig 3.26 a) & b): SHEAR AND DILATION BEHAVIOUR OF 45°-15° ASPERITY SAMPLE UNDER $\sigma_n$= 0.5 MPa**

## 3.4 DEVELOPMENT OF EQUATION-

In this section, the graph between Shear stress vs. ratio of normal stress to crushing strength ($\sigma_n/\sigma_c$) for particular asperity angle are plotted, shear stress is plotted to ($\sigma_n/\sigma_c$) because this is a dimensionless number and then a generalized equation is plotted. It is observed that when single equation is derived for the graph ,the error in the values are more .Therefore attempts are made to minimize the error .It is observed that curve changes behavoiur at 0.2 MPa ,therefore two equations are developed for each curve .

**3.4.1 For 15°-30° asperity sample –**Table below shows the values of $\sigma_n/\sigma_c$ and corresponding values of shear stress found from experiments for 15°-30° asperity sample and then curve is plotted .It is observed that curve follow the equation (33) for normal stress $<$ 0.2 MPa and follow equation (34) for normal stress $\geq$ 0.2 MPa .

**Table No.4:** Values of Shear stress for corresponding values of $\sigma_n/\sigma_c$

| $\sigma_n$(MPa) | $\sigma_n/\sigma_c$ | Experimental Shear Stress(MPa) |
|---|---|---|
| 0.05 | 0.00446 | 0.21 |
| 0.1 | 0.00892 | 0.46 |
| 0.2 | 0.01785 | 0.63 |
| 0.3 | 0.02678 | 0.80 |
| 0.4 | 0.03571 | 0.92 |
| 0.5 | 0.04464 | 1.05 |

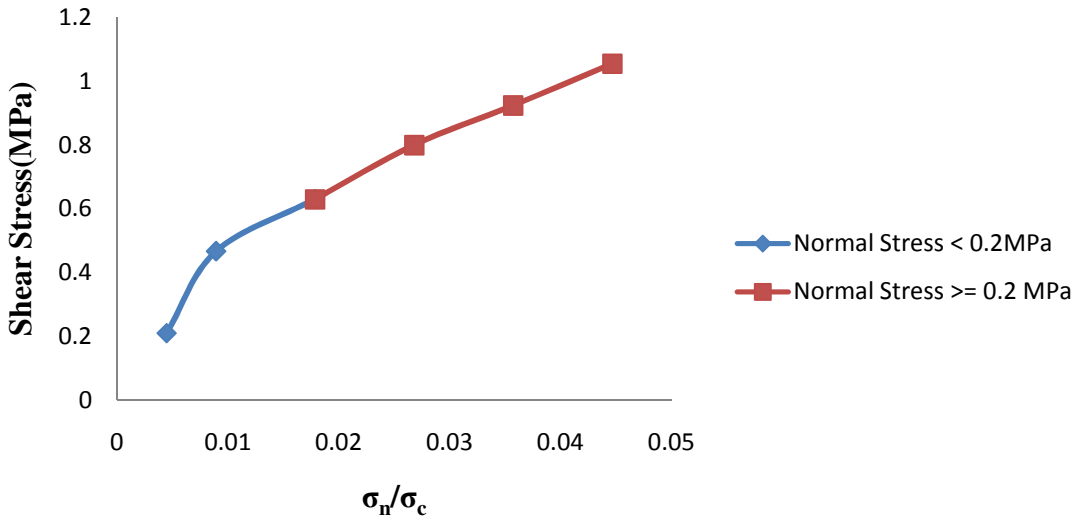


**Fig 3.27: Shows the Variation of Shear Stress vs. $\sigma_n/\sigma_c$ and Equation of curve**

The generalized equation for $\sigma_n < 0.2$MPa is

$$\tau = 0.302 \ln(\sigma_n/\sigma_c) + 1.864 \quad (33)$$

and generelised equation for $\sigma_n \geq 0.2$ MPa is

$$\tau = 0.456 \ln(\sigma_n/\sigma_c) + 2.460 \quad (34)$$

**3.4.2 For 15°-45° asperity angle-** Table below shows the values of $\sigma_n/\sigma_c$ and corresponding values of shear stress found from experiments for 15°-45° asperity sample and then curve is plotted .It is observed that curve follow the equation (35) for normal stress < 0.2MPa and follow equation (36) for normal stress ≥ 0.2MPa .

**Table No.5:** Values of Shear Stress for corresponding values of $\sigma_n/\sigma_c$

| $\sigma_n$(MPa) | $\sigma_n/\sigma_c$ | Experimental Shear Stress(MPa) |
|---|---|---|
| 0.05 | 0.00446 | 0.25 |
| 0.1 | 0.00892 | 0.48 |
| 0.2 | 0.01785 | 0.77 |
| 0.3 | 0.02678 | 1.13 |
| 0.4 | 0.03571 | 1.41 |
| 0.5 | 0.04464 | 1.60 |

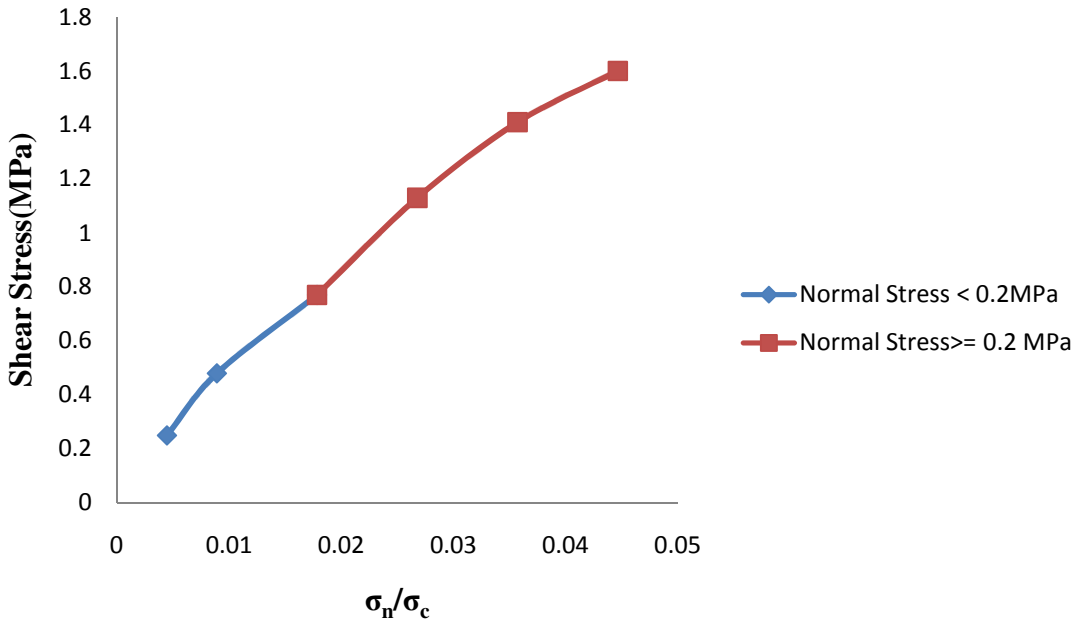


**Fig 3.28: Shows the Variation of Shear Stress vs. $\sigma_n/\sigma_c$ and Equation of curve**

The generalized equation for $\tau$ for $\sigma_n < 0.2$MPa is

$$\tau = 0.375 \ln(\sigma_n/\sigma_c) + 2.269 \quad (35)$$

and generalized equation for $\tau$ for $\sigma_n \geq 0.2$MPa is

$$\tau = 0.911 \ln(\sigma_n/\sigma_c) + 4.439 \quad (36)$$

**3.4.3 For 45°-15° asperity angle –** Table below shows the values of $\sigma_n/\sigma_c$ and corresponding values of shear stress found from experiments for 45°-15° asperity sample and then curve is plotted .It is observed that curve follow the equation (37) for normal stress $< 0.2$ MPa and follow equation (38) for normal stress $\geq 0.2$ MPa.

**Table No.6:** Values of Shear Stress for corresponding values of $\sigma_n/\sigma_c$

| $\sigma_n$(MPa) | $\sigma_n/\sigma_c$ | Experimental Shear Stress(MPa) |
|---|---|---|
| 0.05 | 0.00446 | 0.10 |
| 0.1 | 0.00892 | 0.13 |
| 0.2 | 0.01785 | 0.23 |
| 0.3 | 0.02678 | 0.35 |
| 0.4 | 0.03571 | 0.41 |
| 0.5 | 0.04464 | 0.45 |

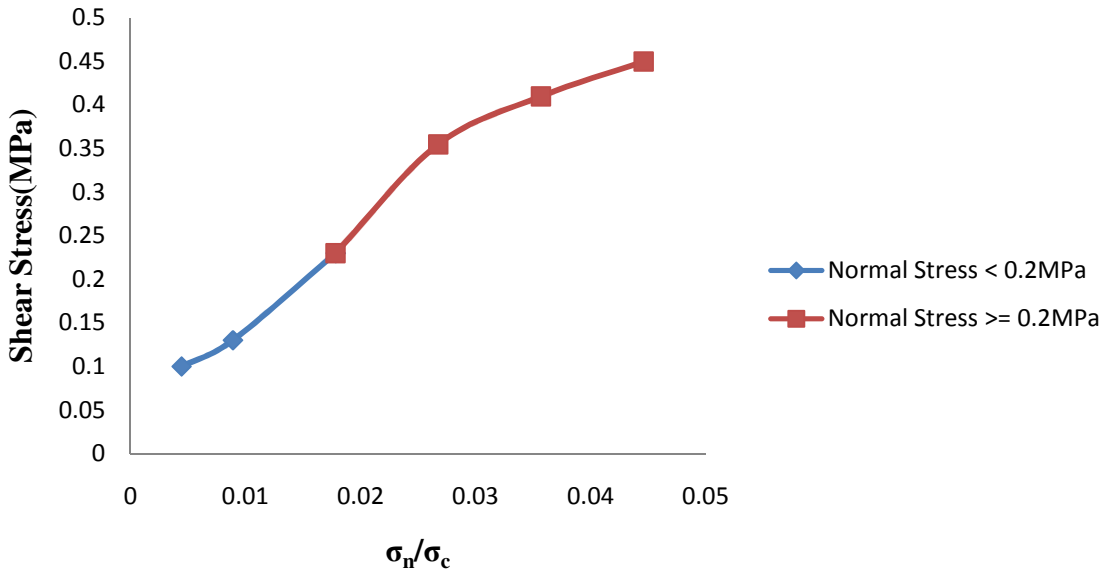


**Fig 3.29: Shows the Variation of Shear Stress vs. $\sigma_n/\sigma_c$ and Equation of curve**

The generalized equation for $\tau$ for $\sigma_n < 0.2$ MPa is

$$\tau = 0.093 \ln(\sigma_n/\sigma_c) + 0.595 \quad (37)$$

and generalized equation for $\tau$ for $\sigma_n \geq 0.2$ MPa is

$$\tau = 0.239 \ln(\sigma_n/\sigma_c) + 1.205 \quad (38)$$

From the all above equations we can observe that all the equations follows logarithmic pattern but the constants are different, therefore we can propose a generalized form of all the different equation which are applicable in all region, which itself be logarithmic in nature so that it will give a very easier way to calculate the shear stress for any asperity sample at any normal stress.

**3.4.4 Generalized equation for satisfying all cases-** The generalized equation for all above cases can be represented by equation shown below:

$$\tau = a \ln\left(\frac{\sigma n}{\sigma c}\right) + b \,, \tag{39}$$

where a and b are the constant whose value depends upon the asperity angle for rock sample and normal stress under which testing is done. It is very difficult to remember different values of a and b for different asperity angle so there is a need to propose the generalized equation for a and b

### i) Value of a and b for $\sigma_n$ = 0.05 MPa, 0.1 MPa and 0.2 MPa-

**Table No.7:** Values of a & b

| i (Facing Angle) | a | b |
|---|---|---|
| 15° | 0.093 | 0.595 |
| 30° | 0.302 | 1.864 |
| 45° | 0.375 | 2.269 |
| | | |

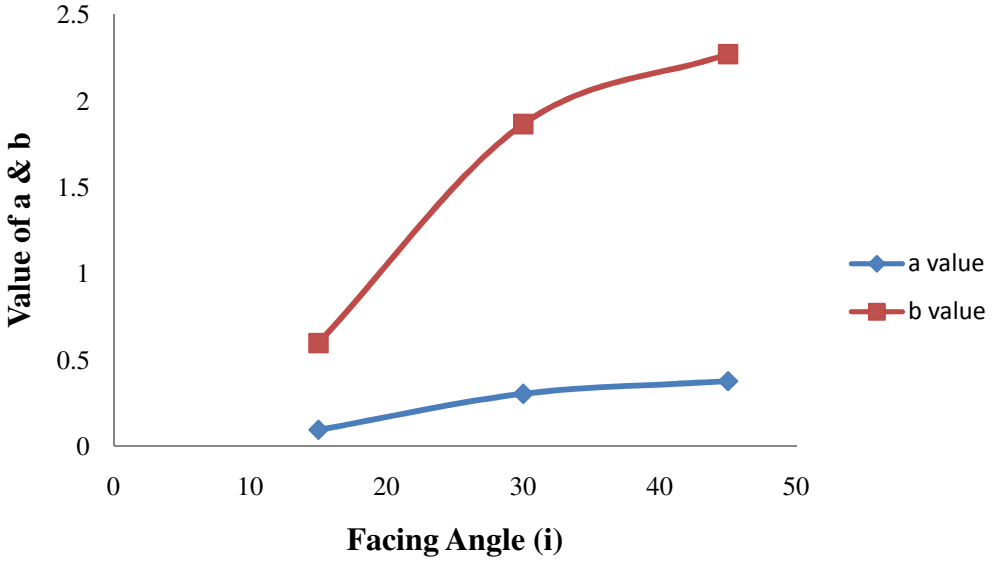


**Fig 3.30: Shows variation of a and b with the Facing Angle (i)**

***Generelized equation for a and b under normal stress = 0.05 MPa, 0.1 MPa, 0.2 MPa –***

From above, we initially assumes that $\tau = a \ln\left(\frac{\sigma n}{\sigma c}\right) + b$, where from above graph general equation for a and b can be given by:

$$a = 0.261 \ln(i) - 0.607 \tag{40}$$

$$b = 1.556 \ln(i) - 3.569 \quad (41)$$

Putting the value of a and b in generalized equation of shear stress, we get final generalized equation for normal stress upto 0.2MPa.

$$\tau = (0.261 \ln(i) - 0.607) \ln\left(\frac{\sigma n}{\sigma c}\right) + (1.556 \ln(i) - 3.569) \quad (42)$$

### ii) Value of a and b for $\sigma_n$ = 0.2,0.3 ,0.4 and 0.5MPa-

**Table No.8:** Values of a & b

| i (Facing Angle) | a | b |
|---|---|---|
| 15° | 0.239 | 1.205 |
| 30° | 0.456 | 2.460 |
| 45° | 0.911 | 4.439 |

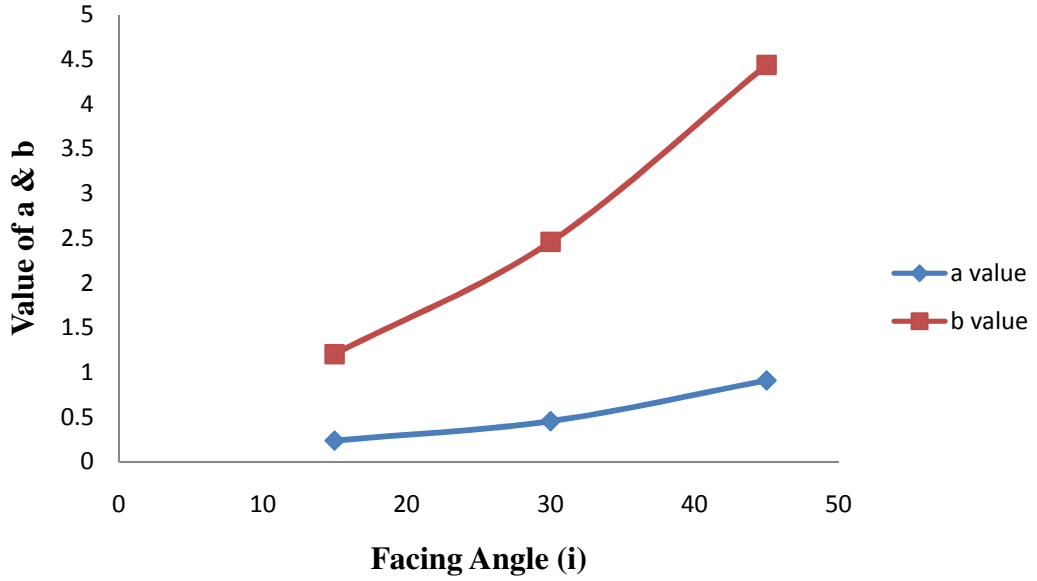


**Fig 3.31: Shows variation of a and b with the Facing Angle (i)**

***Generelized equation for a and b under Normal Stress = 0.2 MPa, 0.3 MPa ,0.4MPa, 0.5MPa –***

From above, we initially assume that $\tau = a \ln\left(\frac{\sigma n}{\sigma c}\right) + b$, where from above graph general equation for a and b can be given by:

$$a = 0.009 (i)^{1.187} \quad (43)$$

$$b = 0.049\ (i)^{1.17} \tag{44}$$

Putting the value of a and b in generalized equation of shear stress, we get final generalized equation for normal stress ≥ 0.2MPa.

$$\boldsymbol{\tau = 0.009\ (i)^{1.187}\ ln\left(\frac{\sigma n}{\sigma c}\right) + 0.049\ (i)^{1.17}} \qquad \boldsymbol{(45)}$$

The above two derived generalized equations *(42)* and *(45)* are both derived for 0.2MPa but Eqn. *(42)* gives accurate results and above 0.2 MPa Eqn.*(45)* is valid because at higher stresses the stress concentration effect will occur.

### 3.4.5 Analysis of Values of Actual Stress, According to Proposed Equation (42) and (45) and error involved-

The generalized equation proposed above contains some error because it is generalized over the wide range of stress and for different asperity angles. First of all shear stress is calculated for particular value of normal stress ,and the shear stress is calculated by our proposed equation and then the percentage error involved is calculated as

$$Error(\%) = \left(\frac{Actual\ stress - Acc.to\ Proposed\ Eqn.}{Actual\ stress}\right) \times 100 \tag{46}$$

Sign of error is neglected because we are concern with the magnitude of the error involved.

**Table No.9:** Values of Actual Stress ,According to formula and error employed

| i(Facing Angle) | Normal Stress($\sigma_n$) | Actual Stress(MPa) | Acc. To Eqn. (46) | Error(%) |
|---|---|---|---|---|
| 15° | 0.05 | 0.10 | 0.10463 | 4.63 |
| 30° | 0.05 | 0.21 | 0.20414 | 2.78 |
| 45° | 0.05 | 0.25 | 0.26235 | 4.94 |
| 15° | 0.1 | 0.13 | 0.17381 | 33.70 |
| 30° | 0.1 | 0.46 | 0.39872 | 14.62 |
| 45° | 0.1 | 0.48 | 0.53028 | 10.47 |
| 15° | 0.2 | 0.23 | 0.24299 | 5.65 |
| 30° | 0.2 | 0.63 | 0.59329 | 5.83 |
| 45° | 0.2 | 0.77 | 0.79821 | 3.66 |
| 15° | 0.3 | 0.35 | 0.35384 | 0.33 |
| 30° | 0.3 | 0.80 | 0.77455 | 3.18 |
| 45° | 0.3 | 1.13 | 1.22422 | 8.33 |
| 15° | 0.4 | 0.41 | 0.41828 | 2.02 |
| 30° | 0.4 | 0.92 | 0.92128 | 0.34 |
| 45° | 0.4 | 1.41 | 1.46164 | 3.65 |
| 15° | 0.5 | 0.45 | 0.46827 | 4.06 |
| 30° | 0.5 | 1.05 | 1.03508 | 1.89 |
| 45° | 0.5 | 1.6 | 1.64580 | 2.85 |

# CHAPTER-4

# COMPARISON OF RESULT

## 4.1 COMPARISION OF PEAK SHEAR STRESS-

The experimental results of shear stress are compared with well known equations of Barton Eqn. (6), Patton's equation (1) and with equation proposed by equation proposed by Shrivastava and Rao (2012) equation (7) so that the conclusion between results obtained from all theories can be made. Table below shows the value of shear strength at different normal stress in different theories.

### 4.1.1 Comparison of Peak Shear Stress for 15°-30° Asperity Sample-

The peak shear stress obtained at different normal stresses for 15°-30° obtained by experiments, Patton's theory and Barton's theory and equation proposed by Shrivastava and Rao (2012) eqn. (7) are plotted so that a comparative study can be done.

**Table No.10:** Values of Peak Shear stress for 15°-30° Asperity Sample

| **Normal Stress (MPa)** | **Experimental Result (MPa)** | **Patton's Eqn. Of $\tau_p$ (MPa)** | **Barton Eqn. of $\tau_p$ (MPa)** | **Shrivastava and Rao (2012)** |
|---|---|---|---|---|
| 0.05 | 0.210 | 0.130 | 0.156 | 0.185 |
| 0.1 | 0.467 | 0.250 | 0.244 | 0.344 |
| 0.2 | 0.630 | 0.510 | 0.396 | 0.605 |
| 0.3 | 0.800 | 0.750 | 0.532 | 0.813 |
| 0.4 | 0.924 | 0.990 | 0.650 | 0.985 |
| 0.5 | 1.055 | 1.270 | 0.777 | 1.130 |

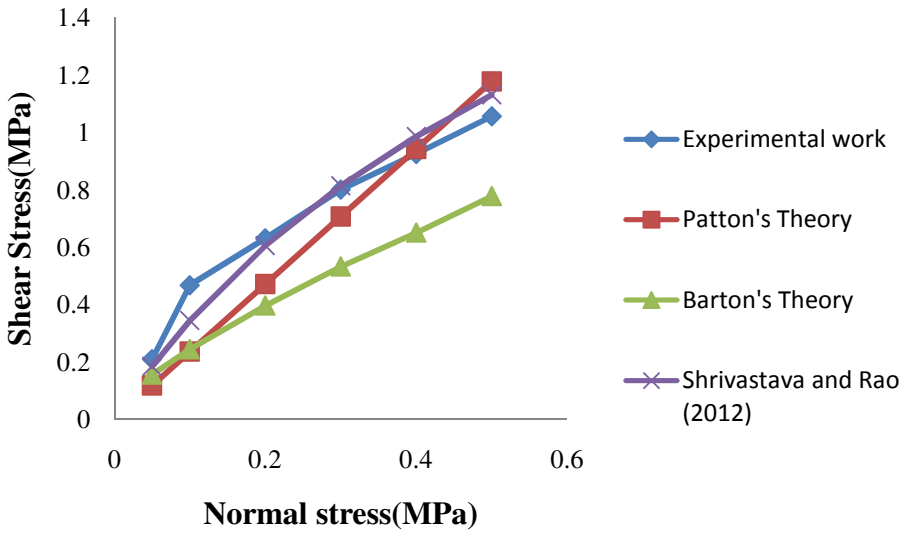


**Fig 4.1: Shows the Comparison of Peak Shear Stress values obtained from Experiment, Patton's, Barton's Theory and with Shrivastava and Rao (2012)**

### 4.1.2 Comparison of Peak Shear Stress for 15°-45° Asperity Sample-

The peak shear stress obtained at different normal stresses for 15°-45° obtained by experiments, Patton's theory and Barton's theory are plotted so that a comparative study can be done.

**Table No.11:** Values of Peak Shear stress for 15°-45° Asperity Sample

| Normal Stress (MPa) | Experimental Result (MPa) | Patton's Eqn. Of $\tau_p$ (MPa) | Barton Eqn. of $\tau_p$ (MPa) | Acc. To Shrivastava2012 |
|---|---|---|---|---|
| 0.05 | 0.25 | 0.355 | 0.476 | 0.099 |
| 0.1 | 0.48 | 0.710 | 0.469 | 0.1943 |
| 0.2 | 0.77 | 1.420 | 0.614 | 0.370 |
| 0.3 | 1.13 | 2.130 | 0.759 | 0.531 |
| 0.4 | 1.41 | 2.846 | 0.896 | 0.680 |
| 0.5 | 1.60 | 3.557 | 1.025 | 0.818 |

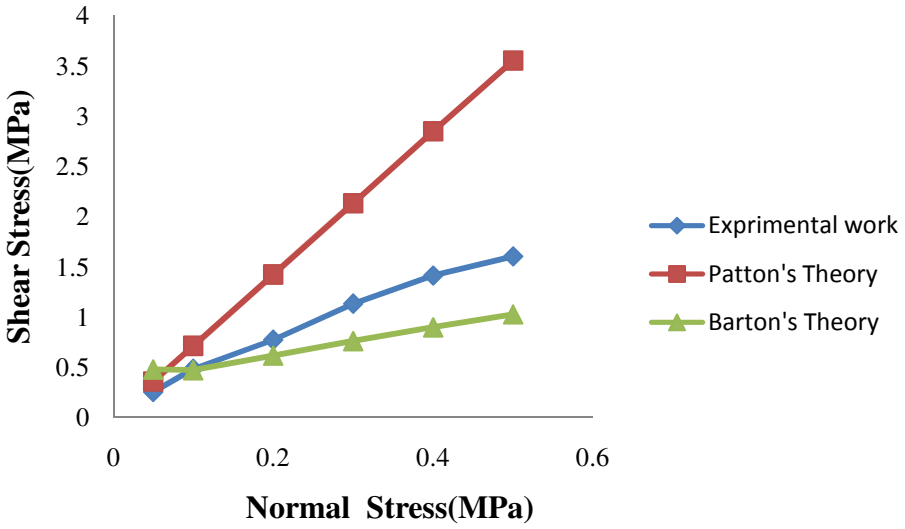


**Fig 4.2: Shows the Comparison of Peak Shear Stress Values obtained from Experiment, Patton's, Barton's Theory**

### 4.1.3 Comparison of Peak Shear Stress for 45°- 15° Asperity Sample-

The peak shear stress obtained at different normal stresses for 45°-15° obtained by experiments, Patton's theory and Barton's theory are plotted so that the comparative study can be done.

**Table No.12:** Values of Peak Shear Stress for 45°-15° Asperity Sample

| **Normal Stress (MPa)** | **Experimental Result (MPa)** | **Patton's Eqn. of $\tau_p$ (MPa)** | **Barton Eqn. of $\tau_p$ (MPa)** |
|---|---|---|---|
| 0.05 | 0.11 | 0.063 | 0.070 |
| 0.1 | 0.13 | 0.127 | 0.129 |
| 0.2 | 0.23 | 0.255 | 0.239 |
| 0.3 | 0.355 | 0.383 | 0.342 |
| 0.4 | 0.41 | 0.511 | 0.441 |
| 0.5 | 0.45 | 0.639 | 0.538 |

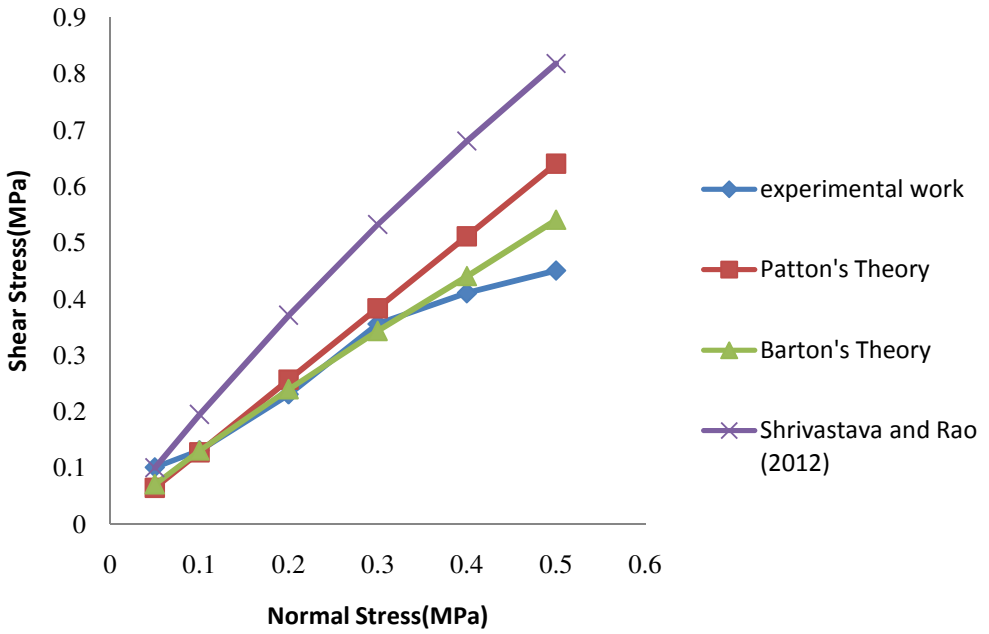


**Fig.4.3: Shows the Comparison of Peak Shear Stress Values obtained from Experiment, Patton's Theory, Barton's Theory and Shrivastava and Rao (2012)**

## 4.2 COMPARISION OF PEAK SHEAR DISPLACEMENT-

The experimental results of peak shear displacement are compared with values obtained from well known of Barton-Bandis (1981) Equation (21). Table below shows the value of Peak shear displacement at different normal stress.

### 4.2.1 Comparison of Peak Shear Displacement for 15°-30° Asperity Sample-

The values of Peak shear displacement of 15°-30° asperity sample obtained experimentally are compared with the values obtained from Barton-Bandis equation and the graph is plotted.

**Table No.13:** Values of Peak Shear Displacement for 15°-30° Asperity Sample

| Normal Stress (MPa) | Experimental Result (mm) | Barton-Bandis Theory (mm) |
|---|---|---|
| 0.05 | 1.76 | 0.74 |
| 0.1 | 3.11 | 0.74 |
| 0.2 | 3.11 | 0.74 |
| 0.3 | 3.21 | 0.74 |
| 0.4 | 3.65 | 0.74 |
| 0.5 | 2.57 | 0.74 |

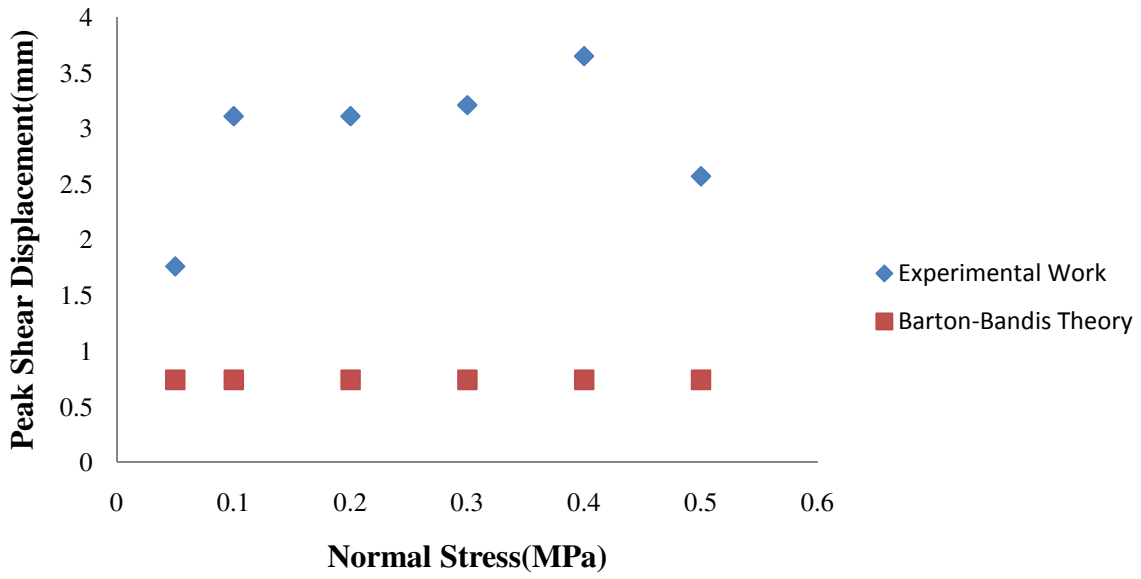


**Fig 4.4: Shows the Comparison of Peak Shear Displacement Values of Experiment and Barton-Bandis Theory**

### 4.2.2 Comparison of Peak Shear Displacement for 15°- 45° Asperity Sample-

The values of Peak shear displacement of 15°-45° asperity sample obtained experimentally are compared with the values obtained from Barton-Bandis equation and the graph is plotted.

**Table No.14:** Values of Peak Shear Displacement obtained for 15°-45° Asperity Sample

| Normal Stress (MPa) | Experimental Result (mm) | Barton Bandis Theory (mm) |
|---|---|---|
| 0.05 | 1.53 | 0.81 |
| 0.1 | 2.75 | 0.81 |
| 0.2 | 3.00 | 0.81 |
| 0.3 | 3.25 | 0.81 |
| 0.4 | 3.63 | 0.81 |
| 0.5 | 3.46 | 0.81 |

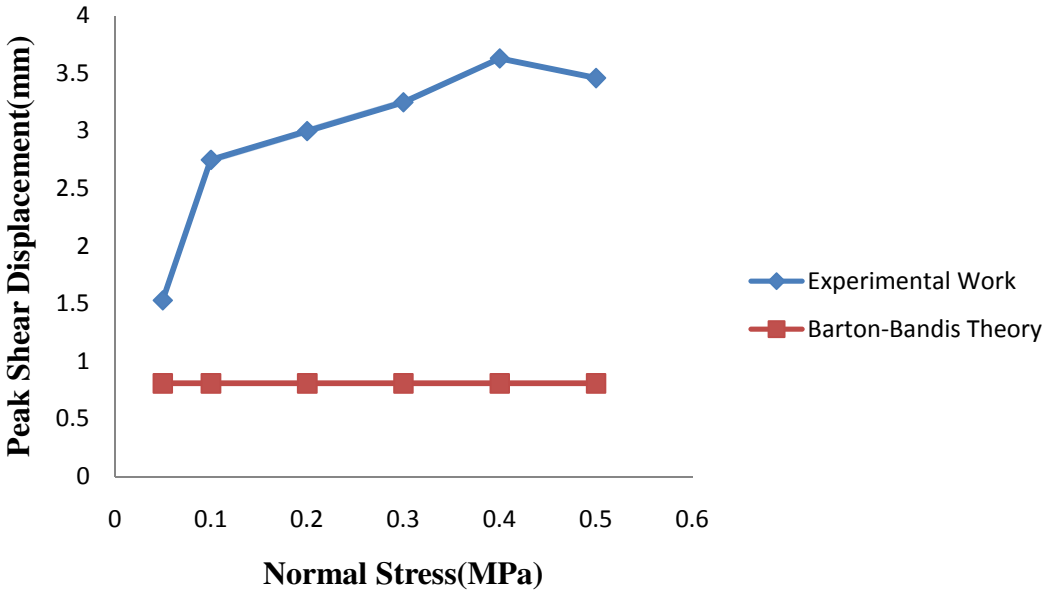


**Fig 4.5: Shows the Comparison of Peak Shear Displacement values of Experiment and Barton-Bandis Theory**

### 4.2.3 Comparison of Peak Shear Displacement for 45° -15° Asperity Sample-

The values of Peak shear displacement of 45°-15° asperity sample obtained experimentally are compared with the values obtained from Barton-Bandis equation and the graph is plotted.

**Table No.15**: Values of Peak Shear Displacement obtained for 45°-15° Asperity Sample-

| Normal Stress(MPa) | Experimental Result(mm) | Barton Bandis Theory (mm) |
|---|---|---|
| 0.05 | 2.63 | 0.59 |
| 0.1 | 0.71 | 0.59 |
| 0.2 | 0.71 | 0.59 |
| 0.3 | 0.90 | 0.59 |
| 0.4 | 1.99 | 0.59 |
| 0.5 | 2.38 | 0.59 |

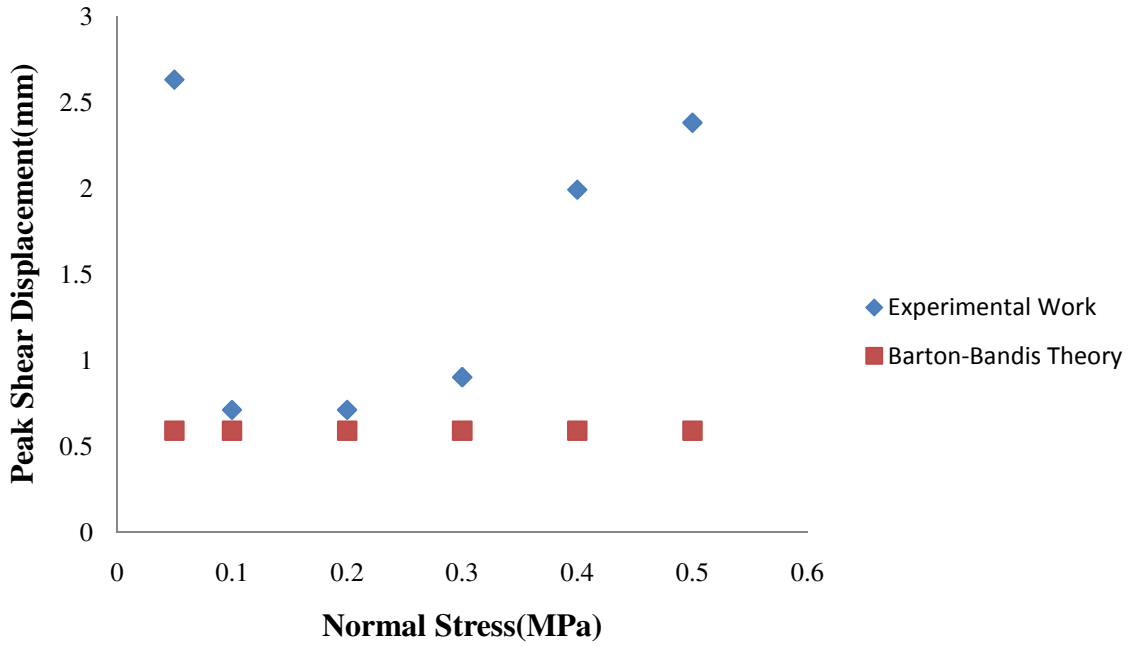


**Fig 4.6: Shows the Comparison of Peak Shear Displacement values of Experiment and Barton-Bandis Theory**

## 4.3 COMPARISION OF PEAK DILATION ANGLE-

Peak secant dilation angle is calculated from experimental results and also from Barton and Choubey (1977) equation (15), then both values are compared and graph is plotted.

Peak secant dilation angle can be determined from experimental values by using the formula as shown below:

$$\delta_{peak} = tan^{-1}\left(\frac{Vertical\ displacement}{Horizontal\ displacement}\right) \quad at\ failure \qquad (47)$$

### 4.3.1Comparison of Peak Dilation angle for 15° -30° Asperity Sample-

The peak secant dilation angle for 15°-30° asperity samples is determined and the values of peak secant dilation angle are also determined from Barton's equation and then the graph is plotted.

**Table No.16 :**Values of Peak Dilation Angle obtained for 15°-30° Asperity Sample

| **Normal Stress $\sigma_n$ (MPa)** | **Experimental values for $d_{s.peak}$ (°)** | **Barton's Eqn. for $d_{s.peak}$ (°)** |
|---|---|---|
| 0.05 | 10.93 | 11.75 |
| 0.1 | 6.42 | 10.24 |
| 0.2 | 6.00 | 8.74 |
| 0.3 | 5.33 | 7.86 |
| 0.4 | 4.69 | 7.23 |
| 0.5 | 4.20 | 6.75 |

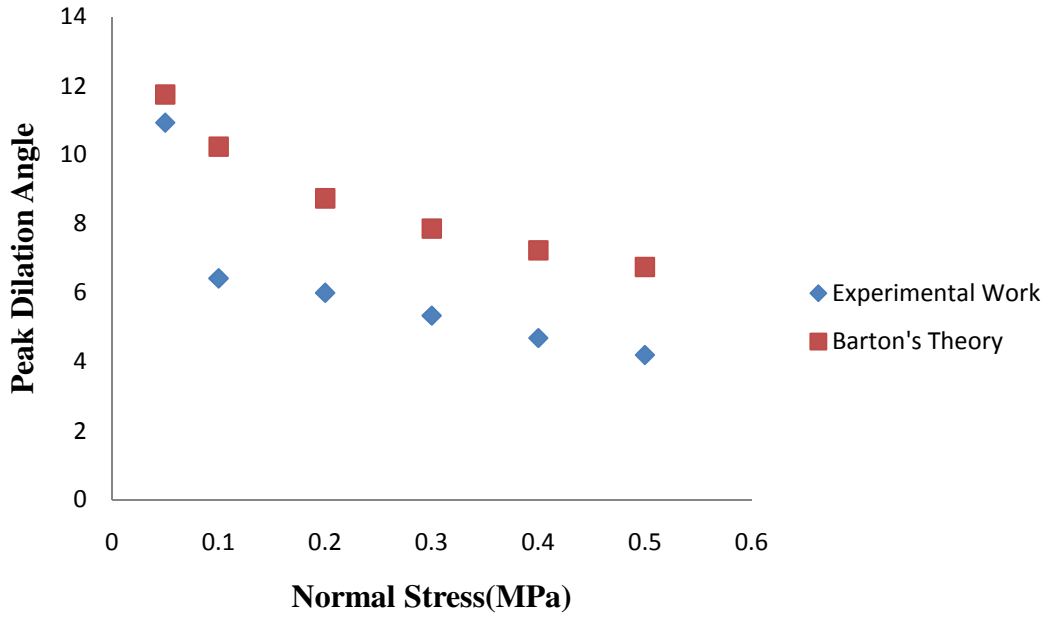


**Fig 4.7: Shows the Comparison of Peak Dilation Angle Values of Experiment and Barton's Theory**

### 4.3.2 Comparison of Peak Dilation Angle for 15° -45° Asperity Sample-

The peak secant dilation angle for 15°-45° asperity sample is determined from experimental values and the values of peak secant dilation angle is also determined from Barton's equation and then the graph is plotted.

**Table No.17:** Values of Peak Dilation Angle obtained for 15°-45° Asperity Sample

| Normal Stress (MPa) | Experimental values for $d_{s.peak}$ (°) | Barton's values for $d_{s.peak}$ (°) |
|---|---|---|
| 0.05 | 12.10 | 15.66 |
| 0.1 | 10.20 | 13.66 |
| 0.2 | 9.45 | 11.65 |
| 0.3 | 6.84 | 10.48 |
| 0.4 | 6.31 | 9.64 |
| 0.5 | 3.32 | 9.00 |

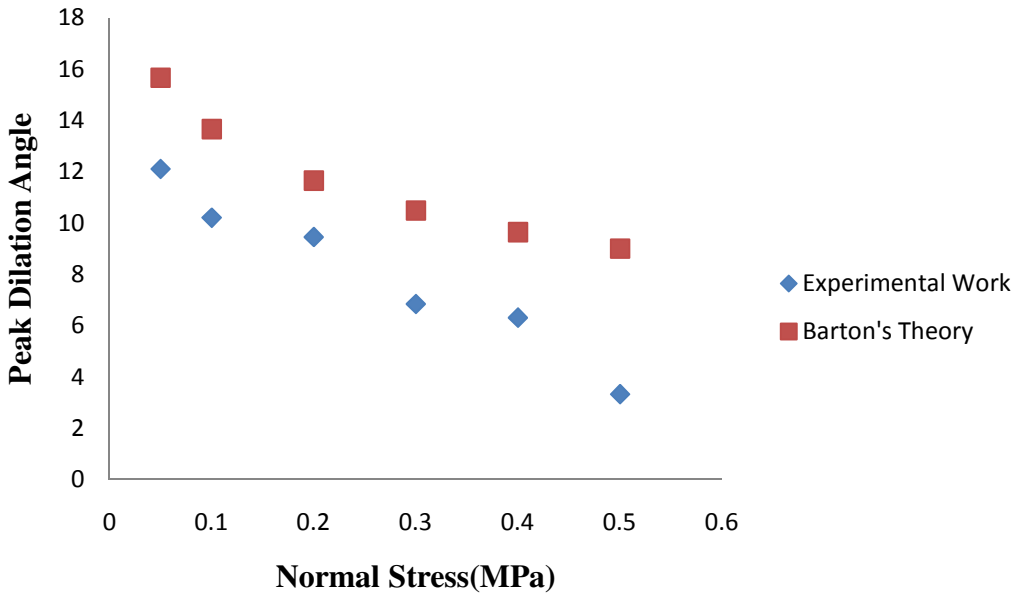


**Fig.4.8: Shows the Comparison of Peak Dilation angle values of Experiment and Barton's Theory**

### 4.3.3 Comparison of Peak Dilation Angle for 45°-15° Asperity Sample-

The peak secant dilation angle for 45°-15° asperity sample is determined from experimental values and the values of peak secant dilation angle is also determined from Barton's equation and then the graph is plotted.

**Table No. 18:** Values of Peak Dilation Angle obtained for 45°-15° Asperity Angle

| Normal Stress (MPa) | Experimental Values for $d_{s.peak}$ (°) | Barton's Values for $d_{s.peak}$ (°) |
|---|---|---|
| 0.05 | 15.10 | 5.87 |
| 0.1 | 7.22 | 5.12 |
| 0.2 | 6.20 | 4.37 |
| 0.3 | 5.10 | 3.93 |
| 0.4 | 4.00 | 3.61 |
| 0.5 | 3.90 | 3.37 |

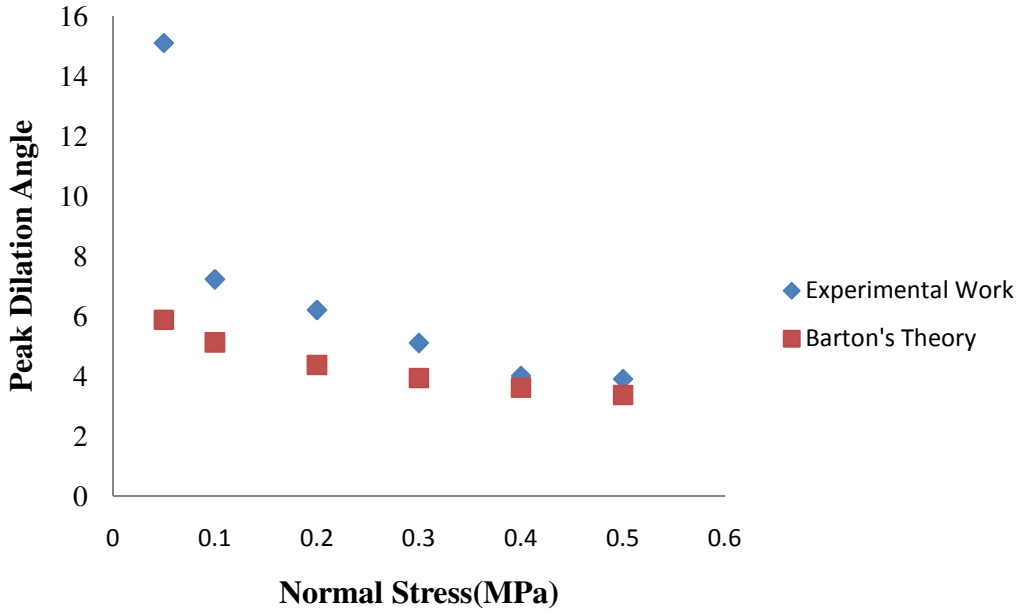


**Fig 4.9: Shows the Comparison of Peak Dilation Angle values of Experiment and Barton's Theory**

# CHAPTER–5

# CONCLUSION AND FUTURE WORK

**5.1 CONCLUSION -** From the experimental result and comparison with the Barton's theory, Patton's theory and with criteria suggested by Shrivastava and Rao (2012) we have following points as Results

1) Peak shear stress increases with the increase in the asperity angle(facing asperity angle) . With increase of facing angle (i) from $15^{\circ}$ to $45^{\circ}$, the peak shear stress increases by 127.27% to 269.2% .This is the fact because as the asperity angle increases it provides greater interlocking.

2) Peak shear stress increases with the increase in the normal stress, it is observed that the peak shear stress increases by 9% to 122.3% with the increase in normal stress from 0.05 MPa to 0.5 MPa.

3) Peak secant dilation angle decreases with increase in normal stress .It is observed that peak secant dilation angle decreases by 2.5% to 47.3% .This is the fact as the normal stress increases the tendency of upward movement will decreases.

4) Peak secant dilation angle for $15^{\circ}$-$30^{\circ}$ and $15^{\circ}$-$45^{\circ}$ asperity sample calculated from experimental values are coming higher than the values obtained from the Barton's equation.

5) Peak secant dilation angle for $45^{\circ}$-$15^{\circ}$ asperity sample calculated form experimental values are lesser than the values obtained from Barton's equation.

6) Peak shear displacement increases with increase in the normal stress upto 79.7% with increase in normal stress upto 0.4 MPa but Peak Shear Displacement decreases suddenly for 0.5 MPa because this is very high Normal Stress at which sample is subjected to the shear stress and vertical stress both so it will leads to the failure of sample at comparatively low value of Peak Shear Displacement.

7) For sample $45^{\circ}$-$15^{\circ}$ asperity sample, the peak shear displacement is large for initial normal stress because $45^{\circ}$-$15^{\circ}$ asperity sample has very less facing angle so it lead to the sliding of sample at low normal stress but as the normal stress increases the peak shear displacement decreases suddenly and then increases with further increase in the normal stress .

8) The experimental result are nearer to the values obtained by Barton's theory, therefore Barton's theory gives more realistic representation.

9) The Generalized equation (42) and equation (45) are developed, which can be used for determination of shear stress of rock of any asperity angle and at any normal stress .

## 5.2 FUTURE WORK-

This study is done under CNL condition but in future this study can be extended for CNS condition,CNS condition gives more realistic result or similar condition as that of the field because in actual condition the stiffness remains constant and if surrounding rock is unable to deform then normal stresses increase inevitably and condition no longer remain CNL. Shear behaviour can also be checked in case of irregular joint having different asperity angle and for joints containing infill material as infill material highly affect the shearing pattern in rock-joints.

# REFRENCES

1. Amadei, B., Saeb, S., 1990. “Constitutive models of rock joints”.International Symposium on Rock Joints. A.A. Balkema, Leon, Norway.

2. Asadollahi, P., Tonon F., 2010. “Constitutive model for rock fractures: Revisiting Barton's empirical model”. Engineering Geology, 11-32.

3. Asadollahi, P., Tonon F., Invernizzi, M.C.A, Addotto, S. 2010, “experimental validation of modified Barton’s model for rock fractures” Rock Mech Rock Eng.

4. Bandis, S.C., Lumsden, A.C. and Barton, N., 1981. “Experimental studies of scale effects on the shear behaviour of rock joints”. 18: 1–21.

5. Bandis, S.C., Lumsden, A.C., Barton, N.R., 1983. “Fundamentals of rock joint deformation” Int. J. Rock Mech. Min. Sci. & Geomech. Abstr. 20 (6), 249–268.

6. Barla, G., Barla, M. 1999, “Continuum And Discontinuum Modelling In Tunnel Engineering”, Scientific Symposium Rock Mechanics and Tunnelling, Zagreb, Croatia.

7. Barton, N., 1972.” A model study of rock joint deformation”. Int. J. Rock Mech. Min. Sci. 9, 570–602.

8. Barton, N., 1973. “Review of a new shear strength criterion for rock joints”. Eng. Geol. 7, 287–332.

9. Barton, N., 1976.” Rock mechanics review: the shear strength of rock and rock joints”.Int. J. Rock Mech. Min. Sci. & Geomech. Abstr. 13, 255–279.

10. Barton, N., Choubey, V., 1977. “The shear strength of rock joints in theory and practice” Rock Mech. 10, 1–54.

11. Barton, N. & Bandis, S. 1982, " Effects of block size on the shear behaviour of jointed rock". Keynote Lecture, 23rd US Symposium on Rock Mechanics, Berkeley, California.

12. Beer G, Meck J. L.,1981, "Infinite domain elements", International Journal Numerical Methods Eng, 17(1): 43–52.

13. Bobet, A., Fakhimi, A., Johnson, S., Morris, J., Tonon F. and Yeung, M.R., 2009, "Numerical Models in Discontinuous Media: Review of Advances for Rock Mechanics Applications", Journal Of Geotechnical And Geoenvironmental Engineering , ASCE / November .

14. Brady, BHG, Wassyng A., 1981, "A coupled finite element—boundary element method of stress analysis", Int J Rock Mech Min Sci Geomech Abst ,pp. 475–85.

15. Cundall, P.A., Hart, R.D., 1992. "Numerical modelling of discontinua". Eng Comput; 9:101–13.

16. Desai, C.S., Fishman, K.L., 1987. "Constitutive models for rocks and discontinuities (joints)". 28th US Symp. on Rock Mechanics, Tuscon, pp. 609–619.

17. Homand, F., Belem, T., Souley, M., 2001. "Friction and degradation of rock joint surfaces under shear loads". Int. J. Numer. Anal. Methods Geomech. 25, 973–999.

18. Homand, F., Lefevre, F., Belem, T., Souley, M., 1999. "Rock joints behaviour under cyclic direct shear tests". In: Amadei, K., Smealie, Scott (Eds.), Rock Mechanics for Industry. Balkema, Rotterdam, pp. 399–406.

19. Indraratna, B. (1990). "Development and application of a synthetic material to simulate soft sedimentary rocks." Geotechnique, Vol. 40, No. 2, pp. 189-200.

20. . Indratna, B., Haque, A. and Aziz, N., 1998, "Laboratory modelling of Shear behaviour of soft joints under CNS condition", Geotechnical and Geological Engineering, pp.17-44.

21. Jing, L. 2003, "A Review Of Techniques, Advances And Outstanding Issues In Numerical Modelling For Rock Mechanics And Rock Engineering", International Journal of Rock Mechanics & Mining Sciences 40, pp. 283–353.

22. Jing, L. and Hudson A, 2002, "Numerical Methods In Rock Mechanics", International Journal of Rock Mechanics & Mining Sciences, pp. 409–427.

23. Jing, L., Stephansson, O., Nordlund, E., 1993. "Study of rock joints under cyclic loading conditions". Rock Mech. Rock Engg. 26 (3), 215–232.

24. Ladanyi, B., Archambault, G., 1970. "Simulation of the shear behaviour of a jointed rock mass". The 11th Symposium on Rock Mechanics, Berkeley, pp. 105–125.

25. Lorig LJ,Brady BGH1984 "A hybrid computational scheme for excavation and support design in jointed rock media ,Preceeding of the symposium Design and Performance of underground excavation .Cambridge British Geotechnical society , .pp.105-12 .

26. Patton, F.D., 1966a . "Multiple modes of shear failure in rock". The 1st Congress of the International Society of Rock Mechanics, Lisbon, pp. 509–513.

27. Perrone N, Kao R. A., 1975, "General finite difference method for arbitrary meshes". Comput Struct , pp.45–58.

28. Rao, K.S. and Shrivastava, A.K., 2011, "Shear behaviour of rock under CNL and CNS condition." Indorock, IIT Roorkee,pp.13-24.

29. Shi, G. H., and Goodman, R. E., 1984, "Discontinuous deformation analysis." Proc., 25th U.S. Symposium on Rock Mechanics, Society of Mining Engineers of AIME, NewYork, 269–277.

30. Shi, G. H., and Goodman, R. E. 1985. "Two dimensional discontinuous deformation analysis." Int. J. Numer. Analyt. Meth. Geomech. 9, pp.541–556.

31. Shi, Goodman, 1988, "Discontinuous deformation analysis—A new numerical model for the statics and dynamics of block systems." Ph.D. thesis. Univ. of California, Berkeley, Calif.

32. Shrivastava, A.K., Rao K.S. and Rathod, G.W. 2012, "Numerical Simulation of Direct Shear Test on Rock-Joint" GSP, ASCE, pp. 2177-2186.

33. Wibowo, J., 1994. "Effect of Boundary Conditions and Surface Damage on the Shear Behaviour of Rock Joints: Tests and Analytical Predictions". University of Colorado at Boulder, Boulder, CO. 200 pp.

34. Zhao, Xingguang,Cai Meifeng,Cai M. (2010)"Rock Dilation on Modeling Failure and Deformation of Hard Rocks". Journal of Rock Mechanics and Geotechnical Engineering, 2 (4): 338–349.

35. ITASCA Consulting Group, Inc. UDEC Manual, 2004.

36. . ITASCA Consulting Group, Inc. 3DEC Manual, 2004.